

1 A novel technique for the humidity dependent calibration of 2 hypoiodous acid (HOI) and iodine (I₂)

3 Lewis Marden¹, Marvin D. Shaw¹, Stephen J. Andrews¹, Maya Zmajkovic¹, Phil Rund², Becky
4 Alexander², Joel Thornton², Andrew Peters³, Peter Karadakov⁴, Lucy J. Carpenter¹

5 ¹Wolfson Atmospheric Chemistry Laboratories, Department of Chemistry, University of York, Heslington, York, YO10 5DD,
6 UK

7 ²Department of Atmospheric and Climate Sciences, University of Washington

8 ³Bermuda Institute of Ocean Sciences, St George's, Bermuda

9 ⁴Department of Chemistry, University of York, Heslington, York, YO10 5DD

10 *Correspondence to:* Lewis Marden (lewis.marden@york.ac.uk), Lucy Carpenter (lucy.carpenter@york.ac.uk), Marvin Shaw
11 (marvin.shaw@york.ac.uk)

12

13 **Abstract.** Hypoiodous acid (HOI) and molecular iodine (I₂) are important precursors of reactive gaseous iodine, which plays
14 an important role in the oxidative capacity of the atmosphere and in aerosol formation in the marine boundary layer. HOI and
15 I₂ are emitted from the ocean surface and recycled on atmospheric aerosol via heterogeneous chemistry. Measurements of
16 these molecules, which are typically present in the marine boundary layer at the low-to-sub part per trillion (ppt) level, are
17 sparse, in part due to difficulties in quantification with a lack of appropriate instrumentation and calibration techniques. A
18 novel calibration technique is developed for HOI via generation from I₂ hydrolysis and then 1:1 conversion of HOI back to I₂
19 through a NaI trap, allowing the sensitivity of HOI to be calculated relative to I₂, which is readily calibrated using a permeation
20 tube system. Using this calibration method, we describe the use of a reduced pressure high resolution chemical ionisation mass
21 spectrometer (CIMS) to characterise the sensitivities of HOI and I₂ over a range of humidities representative of the marine
22 boundary layer and to measure these molecules in the field. At humidities of over 50% RH, the CIMS sensitivity of I₂ is
23 humidity independent whereas HOI exhibits a slight negative humidity dependence. The effect of inlet interactions on HOI
24 and I₂ signals is investigated, with HOI observed to convert to I₂. The implications of these inlet interactions and humidity
25 sensitivities for future ambient measurement configurations are discussed.

26 1 Introduction

27 Iodine species play an important role in atmospheric chemistry and climate. They influence the oxidative capacity of the
28 atmosphere through the destruction of ozone (O₃) (Chameides and Davis, 1980; Solomon et al., 1994; Read et al., 2008; Saiz-
29 Lopez et al., 2014; Sherwen et al., 2016a) and alteration of hydrogen oxides (HO_x) and nitrogen oxides (NO_x) cycles (Simpson

30 et al., 2015; Saiz-Lopez and Von Glasow, 2012). They can also oxidize elemental mercury (Calvert and Lindberg, 2004;
31 Auzmendi-Murua et al., 2014; Lee et al., 2024) and are involved in new particle formation, with iodine oxide radicals (IO),
32 produced during the reaction between O₃ and iodine, self-reacting and further ozonising to form I₂O₅ which can hydrolyse to
33 form HIO₃ (O'dowd et al., 2002; Sipilä et al., 2016; Finkenzeller et al., 2023).

34

35 Of the halogens, iodine has the most profound impact on tropospheric O₃ cycling and significantly modifies the atmospheric
36 response to anthropogenic perturbations of ozone precursor emissions. Global model simulations show that atmospheric iodine
37 chemistry lowers the global tropospheric O₃ burden by 6–20% and reduces O₃ concentrations by several parts per billion (ppb),
38 with significant effects over polluted and populated regions (Saiz-Lopez et al., 2014; Sherwen et al., 2016a; Sherwen et al.,
39 2016b; Wang et al., 2021b; Pound et al., 2023; Caram et al., 2023). The dominant source of atmospheric iodine is from the
40 oceans, primarily from the reaction of O₃ and iodide on the sea surface (Garland et al., 1980; Carpenter et al., 2013; Macdonald
41 et al., 2014), resulting in the emission of molecular iodine (I₂) and hypoiodous acid (HOI). HOI is thought to be the largest
42 source, representing ≈75% of iodine emissions into the troposphere (Sherwen et al., 2016a). In the atmosphere, I₂ and HOI
43 rapidly photolyse, producing reactive iodine radicals that catalytically destroy O₃ (Saiz-Lopez and Von Glasow, 2012; Simpson
44 et al., 2015). This cycle represents a negative feedback mechanism, whereby increased O₃ concentrations are offset by
45 increased iodine emissions (Carpenter et al., 2013; Prados-Roman et al., 2015). In fact, model calculations project that future
46 increases in anthropogenic O₃ will be buffered by iodine (Iglesias-Suarez et al., 2020), which has implications for future air
47 quality. Ice core records have shown that there has been a tripling of atmospheric iodine since 1950 (Cuevas et al., 2018;
48 Legrand et al., 2018), likely due to increased anthropogenic O₃ production. Recent measurements of iodine radicals in the
49 lower stratosphere (Koenig et al., 2020) have also demonstrated the potential for iodine to contribute to stratospheric ozone
50 depletion. Iodine has a far higher O₃ destruction potential than chlorine (Klobas et al., 2021) and has been implicated as a
51 potential reason for the unexplained decrease in extra-polar lower stratospheric O₃ (Koenig et al., 2020), which is a region
52 where O₃ changes exert strong radiative effects on climate (Neale et al., 2025).

53

54 Despite the significance of HOI and I₂ as the main emission source of atmospheric iodine, and of HOI as a sink for the iodine
55 oxide (IO) radical, there have been few measurements of these compounds. Measurements of I₂, which has been detected by
56 both Differential Optical Absorption Spectroscopy (DOAS) and by Chemical Ionisation Mass Spectrometry (CIMS), have
57 typically been restricted to coastal areas (Saiz-Lopez and Plane, 2004; Bitter et al., 2005; Peters et al., 2005; Mahajan et al.,
58 2009; Huang et al., 2010) with only one measurement in the remote ocean region (Lawler et al., 2014). There has so far been
59 only one directly quantified measurement of HOI, by CIMS, also in a coastal region rather than the open ocean (Tham et al.,
60 2021). There are several challenges that contribute to the scarcity of measurements of these molecules. The mixing ratios of
61 iodine compounds are low, in the sub-ppt to 10 ppt range over the ocean, due to their short atmospheric lifetimes (Saiz-Lopez
62 et al., 2012; Lawler et al., 2014). In addition, halogen compounds can undergo heterogeneous chemistry on the surfaces of
63 instrument inlets, resulting in loss or potentially addition of signal (Neuman et al., 2010; Liao et al., 2012; Liao et al., 2014;

64 Le Breton et al., 2017; Peng et al., 2022). Further, there is a lack of highly sensitive and selective measurement techniques and
65 instrumentation to measure and quantify these compounds. Given that reactive halogen chemistry is increasingly being
66 incorporated into global chemistry transport models, there is an urgent requirement for observations to help provide constraints
67 and improve model capabilities.

68
69 Chemical ionisation mass spectrometry is increasingly being used in the measurement of trace atmospheric gases due to its
70 high sensitivity and selectivity, high time-resolution, soft ionisation, and ability to directly measure compounds in the field
71 with minimal sample preparation (Huey, 2007; Lee et al., 2014; Zhang et al., 2023; Riva et al., 2024). Reagent ions are
72 generated and interact with sample molecules in an ion molecule reactor (IMR) to produce analyte ions, such as through charge
73 transfer or adduct formation reactions. Various reagent ions have been used to measure atmospheric halogen species such as
74 SF_5^- to measure HCl and ClONO_2 (Marcy et al., 2005), NO_3^- to measure HIO_3 (Sipilä et al., 2016; Finkenzeller et al., 2023),
75 and SF_6^- to measure bromine and chlorine compounds such as Br_2 , Cl_2 , BrCl , IBr , and BrO (Sjostedt and Abbatt, 2008; Buys
76 et al., 2013; Roscoe et al., 2014). More recently, I^- has been used for a wide range of chlorine and bromine atmospheric species
77 including Cl_2 , Br_2 , ClNO_2 , BrNO_2 , ClONO_2 , ClO , BrO , HCl , HOCl , HOBr , BrCl , and various chlorine-containing OVOCs
78 (Kercher et al., 2009; Lee et al., 2014; Custard et al., 2016; Le Breton et al., 2017; Lee et al., 2018; Priestley et al., 2018).
79 However, the I^- reagent ion is not effective in measuring trace levels of iodine species as they can be formed during the
80 generation of the reagent gas (Wang et al., 2021a). An alternative is to use Br^- as a reagent ion. This has previously been used
81 to measure Cl_2 , HO_2 , H_2SO_4 and HNO_3 (Lawler et al., 2011; Sanchez et al., 2016; Rissanen et al., 2019; Wang et al., 2020)
82 and more recently to detect various iodine species such as I_2 , HOI , ICl and IBr using a chemical ionisation atmospheric pressure
83 interface time-of-flight (CI-API-TOF) mass spectrometer (Tham et al., 2021; Wang et al., 2021a; He et al., 2023). A reduced
84 pressure Br-CIMS has also been developed which can produce analyte ions through an AIM (adduct ionisation mechanism)
85 IMR (Riva et al., 2024). The instrument operates at medium pressures (50–500 mbar) producing low electric fields ($E/N < 10$
86 Td or field-free conditions), which reduces the chances of fragmentation and promotes adduct formation as the primary method
87 of analyte formation. This loses some of the sensitivity compared to higher pressure CIMS instruments due to the reduced
88 numbers of collisions occurring in the IMR. However, this is compensated for with an increased linear range of detected
89 compounds through promotion of adduct formation.

90
91 It has previously been shown that water can form an adduct with halide (I^- , Br^-) reagent ions (R1), which can subsequently act
92 as a reagent ion itself (R3) (Lee et al., 2014; Wang et al., 2021a). The formation enthalpy between a sample molecule and the
93 hydrated reagent ion is lower than with the dry reagent ion (He et al., 2023), and so increasing humidity should result in a
94 decrease in sensitivity, as the proportion of dry reagent ions decreases. However, for small molecules (<8 atoms), increasing
95 humidity has generally been shown to increase sensitivity (Lee et al., 2014; Iyer et al., 2016). This was explained by Quantum
96 Rice-Ramsperger-Kassel (QRRK) theory (Rice and Ramsperger, 1927; Kassel, 1928) which treats the halide adduct cluster as
97 a collection of identical harmonic oscillators (vibrational modes) at the same frequency. On formation of the cluster, the energy

98 produced is distributed amongst the cluster vibrational modes. Not all vibrational modes are considered accessible with
99 experimental evidence suggesting the number of accessible vibrational modes is about half of the total number of vibrational
100 modes (Laidler, 1987). The cluster will fragment if energy above a critical threshold is localised in a single vibrational mode.
101 The rate at which this occurs for a cluster (the decay rate) is calculated by Eq. (1) (Kurtén et al., 2010; Lee et al., 2014).

$$102 \quad k = \nu \frac{j!(j-m+s-1)!}{(j-m)!(j+s-1)!} \quad (1)$$

104 where k is the decay rate (s^{-1}), ν is the average vibrational frequency of the cluster (cm^{-1}), s is the number of accessible
105 vibrational modes, m is the quantised binding energy and j is the quantised total thermal energy of the cluster (binding energy
106 plus thermal energy of the individual molecules). m and j are quantised by dividing their calculated energies (cm^{-1}) by ν .

108 Adding a water molecule to the cluster increases the number of vibrational modes, which decreases the probability that the
109 critical energy threshold is reached in a single oscillator (Kurtén et al., 2010), resulting in a decrease in the decay rate of the
110 newly formed clusters (R4 and R5). Additionally, a lower energy fragmentation pathway is available for the hydrated adduct
111 (R6), which kicks out the water molecule and keeps the sample molecule and reagent ion together.



120 where A is the sample molecule.

121 This kinetic enhancement via the water molecule is in competition with the thermodynamic effect of lower formation enthalpy
122 and will affect different sample molecules to different degrees, requiring the humidity dependence of every molecule of interest
123 to be quantified. Additionally, the humidity dependence will vary between instruments due to differences in IMR conditions
124 and instrument tuning settings.

125 In this work, the ability for the Br-CIMS to detect and quantify the iodine species I_2 and HOI is demonstrated, and the impact
126 of changing humidity on the instrument sensitivity to these molecules is quantified.

130 2 Methods

131 2.1 Bromide Time-of-Flight Chemical Ionisation Mass Spectrometry (CIMS)

132 The measurement of I₂ and HOI were performed using a Vocus S Chemical Ionisation Time-of-Flight (CI-TOF) Mass
133 Spectrometer (Tofwerk, Switzerland), a high resolution (R ≈ 5000) instrument that can produce Br⁻ reagent ions and Br-adduct
134 analyte ions through a Vocus Aim reactor. The operational principles of the instrument and the AIM reactor are described in
135 detail by Riva et al. (2024).

136
137 The Br⁻ reagent ions are generated by passing 0.25 SLPM ultra-high purity N₂ gas over a permeation tube held at 80 °C
138 containing >99% benzene, C₆H₆, and trace amounts of bromoethane, C₂H₅Br. This gas mixture is passed into a vacuum
139 ultraviolet (VUV) ion source where UV light is emitted from a Kr lamp at 116.487 nm and 123.584 nm which is absorbed by
140 the benzene, generating photoelectrons (R7) (Ji et al., 2020; Breitenlechner et al., 2022). These photoelectrons react with the
141 C₂H₅Br, generating Br⁻ ions (R8) (Riva et al., 2024).



145
146 The Br⁻ reagent ions are passed into an ion-molecule reactor (IMR) where they are joined by 1.8 SLPM of sample gas which
147 has been passed into the sampling inlet and through a 0.475 mm critical orifice. The IMR is temperature controlled at 50 °C
148 and pressure controlled at 50 mbar using a vacuum pump (IDP3, Agilent Technologies). The Br⁻ reacts with sample molecules
149 to form adduct ions. These are drawn through another critical orifice and travel through four differentially pumped chambers
150 which remove neutral molecules and focus the ions into a narrow beam before entering the drift region of the time-of-flight
151 (ToF) chamber. Ions in the TOF chamber are extracted in discrete packets at a frequency of 18.02 kHz and converted into
152 mass spectra using an MCP detector with a preamplifier over a range of 7–510 Th. The extracted packets are averaged over a
153 period of 1 second which is also the speed of data collection. Data averaging, mass calibration, peak assignment, peak fitting
154 and peak integration were all performed using the software package Tofware (version 4.0.1, Aerodyne Research Inc.) used in
155 Igor Pro 9 software (Wavemetrics). This data was then exported and analysed further using the R language for statistical
156 computing (R Core Team).

157 2.2 Humidity generation

158 The calibrations performed in this work were made over a humidity range from near complete dryness to almost 100% RH in
159 order to be able to correct for effects caused by variations in ambient humidity in field measurements. This was achieved by
160 humidifying the N₂ gas entering the instrument to various degrees using an in-house dynamic liquid calibration unit (LCU).
161 The operation of this liquid calibration system has been described elsewhere (Yeoman et al., 2022) but is briefly covered here.

162 The LCU is comprised of a proportional liquid-gas mixing valve (Bronkhorst) which controls the mass flow of liquid measured
163 by a mini-Coriolis flow meter (Bronkhorst). It introduces a mass flow controlled zero-air dilution gas to aerosolize and fully
164 evaporate the liquid into a temperature-controlled mixing region. The liquid is pressurized without gas contact, using a custom-
165 built pneumatic cylinder with wetted materials of glass and PTFE.

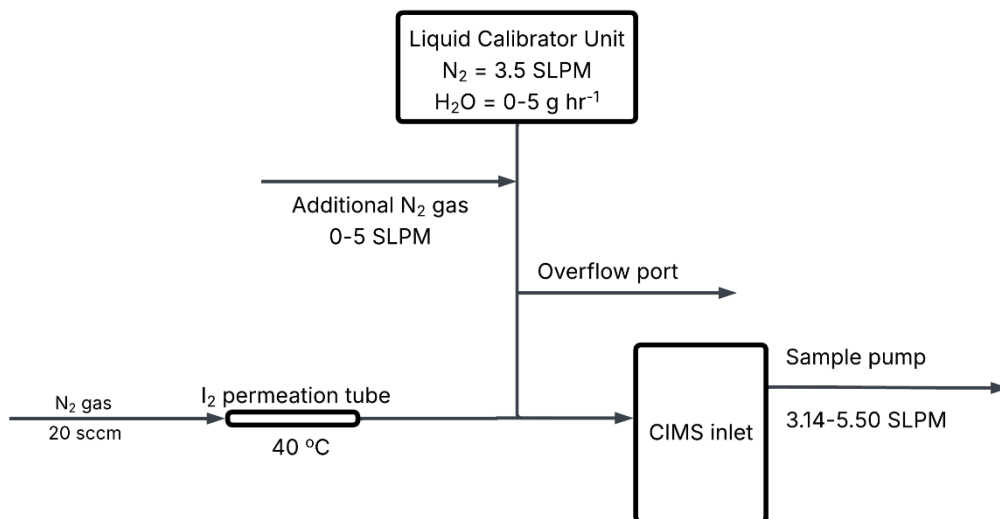
166
167 The gas output of the LCU was maintained at 3.5 SLPM and the water concentration ranged from 0–5 g h⁻¹. During the I₂
168 calibrations, an additional flow of N₂ gas was used to further increase the gas output. The tubing between the LCU outlet and
169 the additional flow was heated to prevent saturation and condensation of the water vapour.

170 **2.3 Calibration setup**

171 **2.3.1 I₂ calibration**

172 An I₂ permeation tube was constructed by adding solid I₂ crystals (99.99%, Sigma-Aldrich) into a ¼” o.d. thin-walled PFA
173 tube with the ends heat sealed closed. The permeation tube was held in a temperature-controlled permeation holder at 40 °C.
174 The temperature variation in the holder was minimal, at ± 0.1 °C, and is included in the uncertainty calculation. The permeation
175 tube was continuously swept by 20 sccm high-purity oxygen-free N₂ gas. The emission rate was calculated gravimetrically by
176 measuring the mass of the permeation tube over a period of 6 months. Measurements were taken on average every 3 weeks
177 with each data point representing the average of 6 sequential mass measurements, as shown in Fig. A1. The emission rate was
178 calculated from the gradient of Fig. A1 and corresponds to an emission rate of 34.7 ± 0.21 ng min⁻¹ with little variation seen
179 during the measurement period.

180
181 A schematic of the I₂ calibration setup is shown in Fig. 1. Humidified N₂ gas from the LCU was used to dilute the permeation
182 gas flow and the CIMS internal sample pump was used to sample this diluted I₂ permeation gas. Before mixing with the
183 permeation gas, the dilution gas was first split, with some diluting the I₂ permeation gas and some passing through an overflow
184 port. The amount of dilution gas mixing with the permeation gas depends on how much flow the CIMS sample pump pulls
185 towards the instrument. By changing this sample flow rate and hence the dilution of the permeation gas, the concentration of
186 I₂ was altered, allowing for the construction of calibration curves at different humidity levels. Concentrations of I₂ generated
187 during the calibrations ranged from 1–3 x 10¹⁰ molecules cm⁻³ (600–1000 ppt at SATP).



188

189 **Figure 1: Schematic of the I₂ calibration setup.**

190 **2.3.2 HOI calibration**

191 HOI was generated from the hydrolysis of I₂ (R9) in an experimental setup similar to that previously developed for the
 192 generation of HOBr in a study by Liao et al. (2012). 500 sccm of N₂ gas was passed over the same I₂ permeation tube from the
 193 I₂ calibration and mixed with 500 sccm N₂ gas which had been humidified by passing through a bubbler containing Milli-Q
 194 water. This was passed over wetted AgNO₃ crystals (99% Fluorochem) in a 9.5 cm long ½" o.d. PFA tube. A small aqueous
 195 layer forms on the AgNO₃ crystal surface, in which I₂ hydrolysis occurs (R9). The AgNO₃ reacts with the generated I⁻ and H⁺
 196 (R10–12), pushing the (R9) equilibrium in favour of HOI production.

197



202

203 The resulting I₂ and HOI gas mixture was diluted by humidified N₂ gas from the LCU before being drawn into the CIMS at a
 204 flow rate of ≈ 4.1 SLPM. The AgNO₃ reactor tube and instrument inlet were wrapped in heating tape and heated to 50 °C to
 205 avoid HOI loss to the tube and inlet walls. The quantification of HOI is achieved by the inclusion of a trap containing sodium
 206 iodide (NaI) crystals (99%, Sigma-Aldrich). When the trap is in place, HOI is converted back into I₂ (R13).

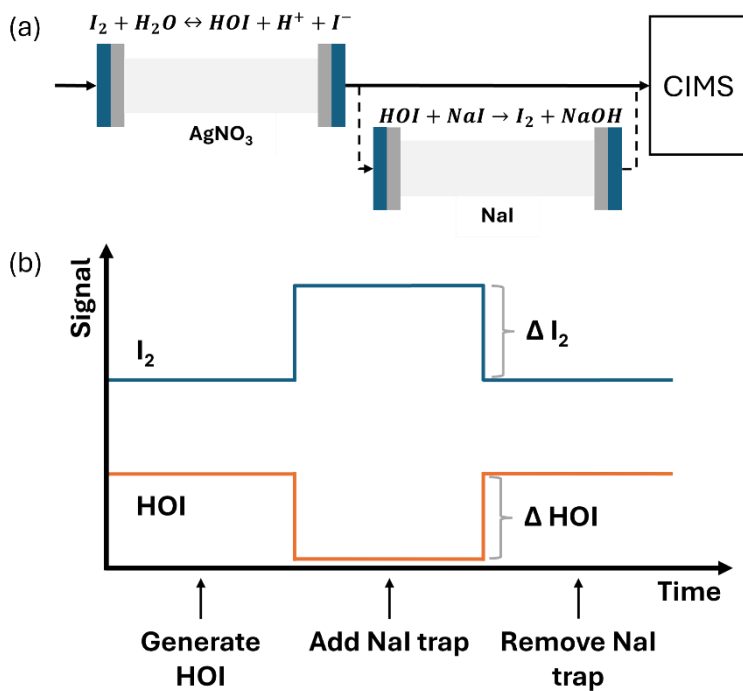
207



209

210 The sensitivity of HOI relative to I_2 was found by comparing the HOI signal loss and I_2 signal gain from R13. A 1:1 conversion
211 of HOI to I_2 was assumed, consistent with the approach of Liao et al. (2012) for the equivalent HOBr–Br₂ system. Figure 2
212 shows the simplified schematic of the calibration setup and an idealised example of the relative change between I_2 and HOI.
213 As water is required in the HOI generation step, the calibrations are performed at high humidity. Lowering the humidity of the
214 N₂ gas should allow for lower humidity calibrations, but this will reduce the yield of HOI produced by (R9), making it more
215 difficult to observe the change in I_2 signal.

216



217

218 **Figure 2: (a) A simplified schematic of the HOI calibration setup with reactions shown for HOI generation and destruction. (b) An**
219 **idealised example of the change in HOI and I_2 signal in the CIMS on addition and removal of the NaI trap.**

220 2.4 Field measurements at Tudor Hill Marine Atmospheric Observatory, Bermuda

221 The CIMS instrument was deployed during the Bermuda boundary Layer Experiment on the Atmospheric Chemistry of
222 Halogens (BLEACH) field campaign in June 2022. The instrument was stationed at the Tudor Hill Marine Atmospheric
223 Observatory (THMAO) on the west coast of the island of Bermuda (32.26° N, 64.88° W). At this site, the instrument was
224 placed on top of a temporary sampling tower at 10 metres above ground level and 40 metres above sea level. The ion source
225 gas was supplied by an air compressor connected to a nitrogen membrane and connected to the instrument by ¼" stainless
226 steel tubing. The instrument was contained in an air-conditioned water-resistant enclosure and located at the top of the tower,
227 minimising the potential for inlet effects to occur. The sample inlet was a short (15 cm, ½ in. outer diameter) length of PFA

228 tube. A PTFE guard was placed at the entrance of the inlet tube, with an opening at the bottom, orientated 90° to the inlet. This
229 allowed air to enter at a 90° bend and continue to the instrument while reducing the number of particles entering the CIMS as
230 they impact onto the inlet walls. The sampling rate was 4.1 L min⁻¹, resulting in an inlet residence time of 0.59 s. The Reynolds
231 number was 155, indicating laminar flow once the air was past an 8.5 cm entrance length.

232 2.5 Quantum chemical calculations

233 Quantum chemical calculations were used to find the vibrational frequency, binding energy and number of vibrational modes
234 for the adducts I₂.Br⁻ and HOI.Br⁻. These were performed using Gaussian 16, Revision C.02 (Frisch et al., 2019), including all
235 electrons in the correlation calculations through “MP2(Full)” and “CCSD(T,Full)”. The geometries of the adducts were
236 optimised at the MP2 level and then single-point energies were calculated, at these geometries, at the CCSD(T) level. All
237 geometry optimisations were carried out under the “VeryTight” convergence criteria, and the optimised geometries were
238 confirmed as local minima through subsequent frequency calculations. All calculations used the standard aug-cc-pVTZ basis
239 set for all atoms except iodine, and the aug-cc-pVTZ-PP ECP basis from the Basis Set Exchange (Pritchard et al., 2019) for
240 iodine. We refer to this combination as “aug-cc-pVTZ-PP”. Binding enthalpies were obtained by adding together the energy
241 difference E (complex) – E (reactants) at the CCSD(T) level to the corresponding difference between the thermal corrections
242 to the enthalpy at the MP2 level (the thermal corrections to the enthalpy involve vibrational contributions, hence the need to
243 have these at the level at which the geometries were optimised). The values are shown in Table 1.

244
245 **Table 1: The calculated vibrational frequencies, binding energy, total thermal energy and vibrational modes of the I₂.Br⁻ and**
246 **HOI.Br⁻ clusters. The decay rate is found using Eq. (1).**

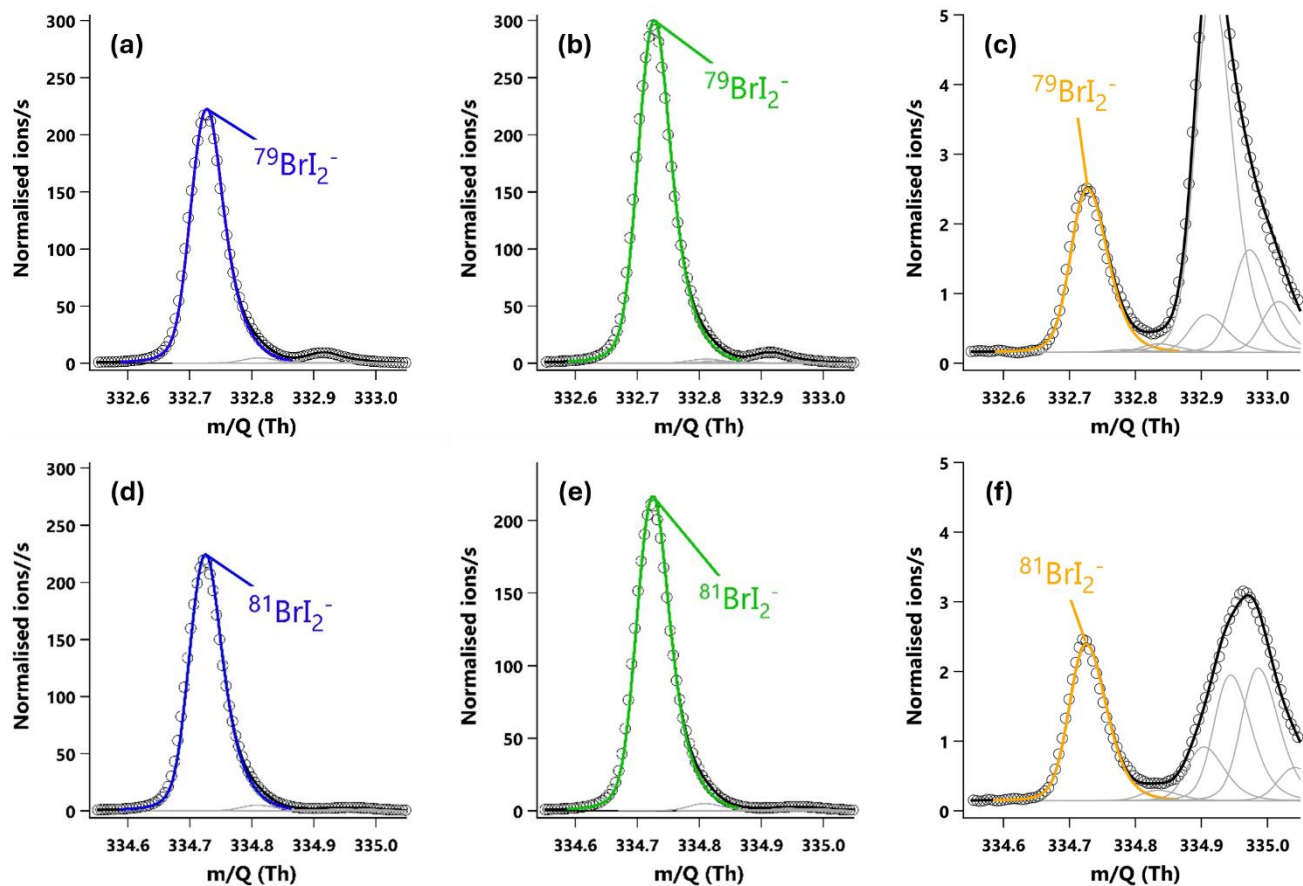
Cluster	Vibrational frequency / Hz	Binding energy / kcal mol ⁻¹	Total thermal energy / kcal mol ⁻¹	Vibrational modes (accessible)	Decay rate / s ⁻¹
I ₂ .Br ⁻	3.06 × 10 ¹²	30.8	33.5	4 (2)	2.66 × 10 ¹¹
HOI.Br ⁻	1.19 × 10 ¹³	24.3	27.1	6 (3)	2.38 × 10 ¹¹

248 3. Results and Discussion

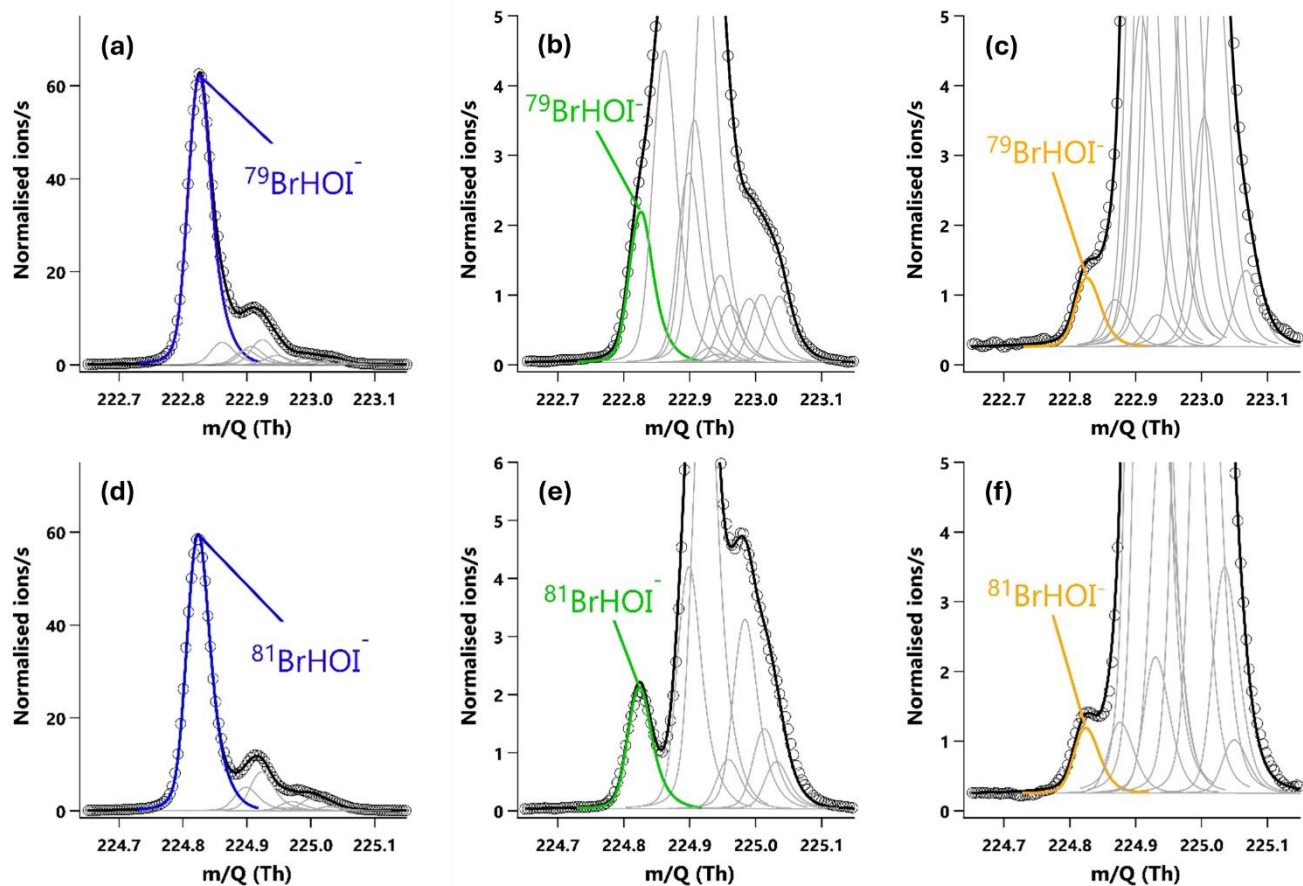
249 3.1 Detection of iodine compounds

250 I₂ and HOI were detected as adducts with Br⁻, with the two I₂.Br⁻ isotopes observed at m/Q 332.73 and 334.73 Th and the two
251 HOI.Br⁻ isotopes at 222.83 and 224.83 Th. The single peak mass spectra fits for I₂ are shown in Fig. 3, and in Fig. 4 for HOI,
252 taken from an HOI calibration experiment and of ambient air at Tudor Hill, Bermuda. At the instrument resolution of 5000,
253 the high mass defect of the I₂.Br⁻ adduct allows it to be clearly differentiated from other peaks even during ambient conditions

254 at low mixing ratios. The HOI.Br⁻ adduct has a smaller mass defect, and subsequently has more overlap with interferent peaks.
 255 During the HOI generation stage of the calibration (Fig. 4a), the HOI signal is significantly greater than any interferent peaks.
 256 However, on addition of the NaI trap (Fig. 4b), or during ambient measurements (Fig. 4c), the HOI signal overlaps with other
 257 interferent peaks. Despite this, the resolution is sufficient for Tofware's multi-peak fitting algorithm (Stark et al., 2015) to
 258 identify HOI even at very low mixing ratios. The signal can be further verified by examining the fit of the HOI isotope peak
 259 (Fig 4. d–f), calculated by the Tofware software. Detection limits during field conditions are discussed in Sect. 3.7.
 260



261
 262 **Figure 3: 20-minute averaged high resolution single peak mass spectra fits for the molecular ion peak (a,b,c) and primary isotope**
 263 **peak (d,e,f) for I₂. The signal intensities correspond to mixing ratios of (a) 190.2 ppt, (b) 254.0 ppt and (c) 1.37 ppt. (a, d) The I₂**
 264 **signal during an HOI calibration run without the NaI trap. (b, e) The I₂ signal during an HOI calibration run on addition of the NaI**
 265 **trap. (c, f) Ambient air measurements of I₂ in a high humidity environment.**



266

267 **Figure 4: 20-minute averaged high resolution single peak mass spectra fits for the molecular ion peak (a,b,c) and primary isotope**
 268 **peak (d,e,f) for HOI. The signal intensities correspond to mixing ratios of (a) 60.8 ppt, (b) 2.2 ppt and (c) 0.87 ppt. (a, d) The HOI**
 269 **signal during an HOI calibration run without the NaI trap. (b, e) The HOI signal during an HOI calibration run on addition of the**
 270 **NaI trap. (c, f) Ambient air measurements of HOI in a high humidity environment.**

271 3.2 Signal normalisation

272 The I₂ and HOI adducts are formed from a pseudo first order reaction between the sample molecules and the Br⁻/H₂OBr⁻
 273 reagent ions, and the adduct signal intensity is proportional to the reagent ions available. During experiments, the quantity of
 274 available reagent ions fluctuates over time. This can be due to variations in the efficiency of the ion source in generating the
 275 reagent ions, or with slight changes within the instrument. This variation can be corrected for by normalising the analyte signal
 276 against the sum of the reagent ions measured by the instrument, shown in Eq. (2). For CIMS instruments, the normalised signal
 277 is typically reported per million reagent ions, with units of normalised counts per second per million reagent ion counts per
 278 second (ncps). It has been reported that normalisation can compensate up to 50% reagent ion depletion from sample molecules
 279 (Riva et al., 2024).

280

281
$$\text{Normalised signal (ncps)} = \frac{A \cdot \text{Br}^- \text{ (cps)}}{\text{Br}^- \text{ (cps)} + \text{H}_2\text{OBr}^- \text{ (cps)}} * 10^6 \quad (2)$$

282

283 where A is the sample molecule.

284 3.3 I₂ humidity dependence

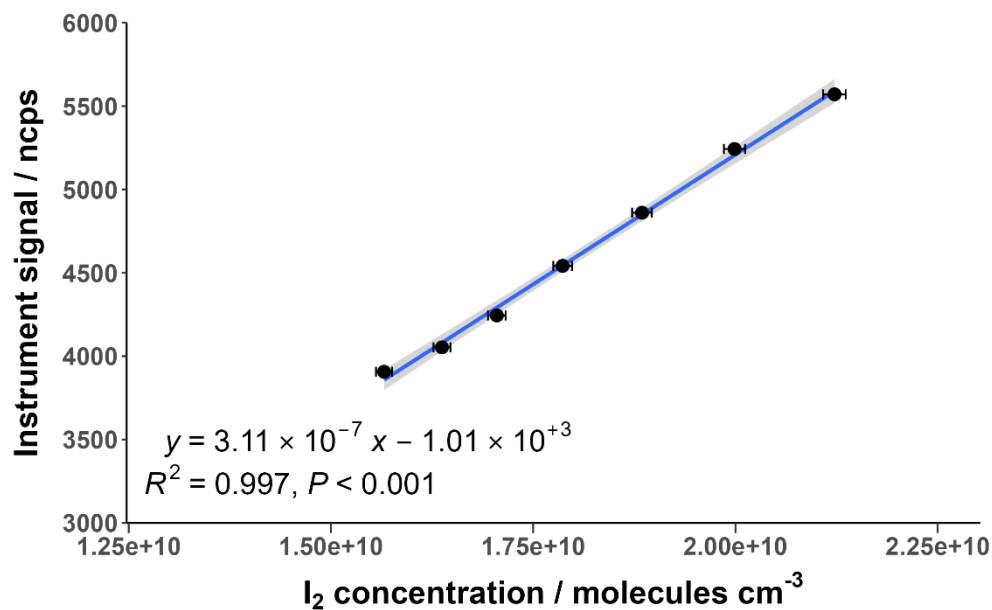
285 The humidity of the instrument IMR, where the reagent ion collisions occur, is not directly measured but has been related to
286 the sample relative humidity (Wang et al., 2021a; He et al., 2023) and/or vapour pressure of water (Lee et al., 2014; Lee et al.,
287 2018). An alternative method is to use the ratio between the first reagent ion water cluster, H₂OBr⁻, and the dry reagent ion,
288 Br⁻ (Dörich et al., 2021), Eq. (3). This has the advantage of not requiring further equipment to measure humidity levels during
289 calibrations and accounts for any changes that may occur when the gas flows through the inlet. The so-called “water ratio” is
290 used hereon to represent humidity. The water ratio is compared against absolute humidity measured during the BLEACH
291 campaign in Fig. A4. Previous studies have shown that IMR temperature can impact the proportions of the hydrated and dry
292 reagent ions, though this has been performed over a wide range of temperatures (Robinson et al., 2022). Fig. A4 shows that
293 there was little variation in the IMR temperature (±0.6 °C) and pressure (±0.35 mbar) during the BLEACH campaign and that
294 these changes did not noticeably affect the water ratio at different humidities.

295

296
$$\text{water ratio} = \frac{\text{H}_2\text{OBr}^- \text{ (cps)}}{\text{Br}^- \text{ (cps)}} \quad (3)$$

297

298 I₂ calibrations were performed at a range of different humidities generated by changing the water mass supplied by the LCU.
299 The range of I₂ concentrations for each humidity was between 1–3 × 10¹⁰ molecules cm⁻³; about two orders of magnitude higher
300 than what would typically be observed in the atmosphere. Ideally, the concentration range would be comparable to atmospheric
301 levels, but limitations in the amount of gas dilution and water mass flow restricted the minimum concentrations that could be
302 used. Low pressure CIMS instruments reportedly have large linear ranges, particularly when normalising to the reagent ion
303 (Riva et al., 2024), and so it is assumed in this work that the calibration range is within the linear range of the instrument. The
304 I₂ sensitivity was determined by calculating the gradient of the calibration curves with units of ncps cm³ molecules⁻¹. The
305 instrument response over the calibration range demonstrated a high degree of linearity, an example of which is shown in Fig.
306 5.

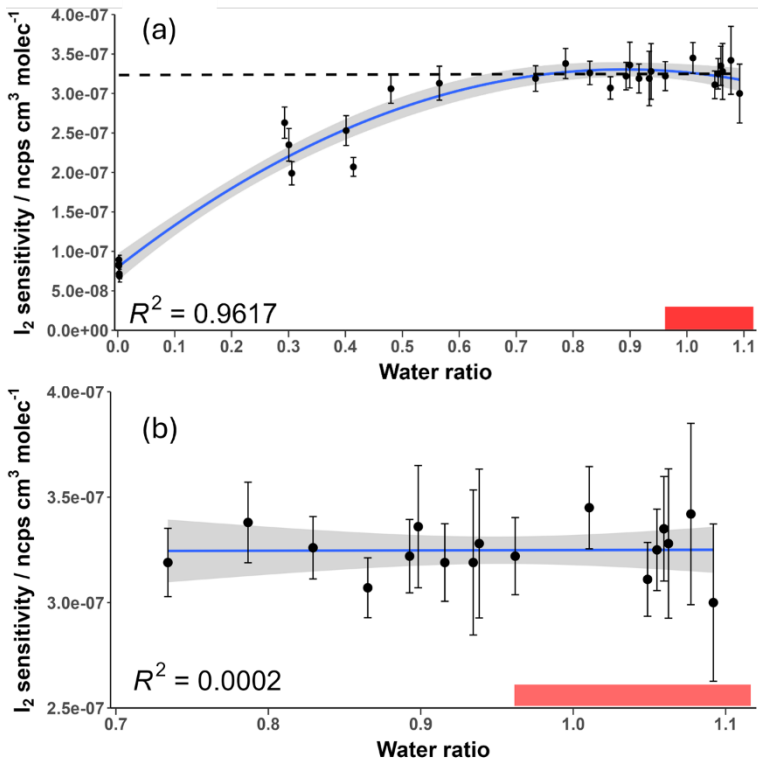


307

308 **Figure 5: Normalised instrument signal against I₂ concentration for an example calibration at a water ratio of 1.05. The shaded area**
 309 **represents the 95% confidence interval of the fitted curve. Error bars indicate the calculated propagated uncertainty of the I₂**
 310 **concentration, shown in Sect. 3.5.**

311

312 The change in I₂ sensitivity at different humidities is demonstrated in Fig 6. Above a water ratio of ~0.7, the sensitivity of I₂
 313 is effectively humidity-independent with a sensitivity of $3.25 \times 10^{-7} (\pm 6.30 \times 10^{-9})$ ncps cm³ molecules⁻¹. This is four times more
 314 sensitive than the average sensitivity of $7.92 \times 10^{-8} (\pm 3.18 \times 10^{-9})$ ncps cm³ molecules⁻¹ at near dryness (average water ratio =
 315 0.0022), which can be attributed to the stabilising effect of the H₂O molecule on the formed adduct. As humidity is increased,
 316 this stabilising effect is balanced out by more adduct formation occurring via the BrH₂O⁻ reagent ion, which is a less exothermic
 317 reaction (Wang et al., 2021a). There is also an increase in the formation of the second water cluster, Br(H₂O)₂⁻, at very high
 318 humidities, shown in Fig 7. There appears to be no literature on whether this cluster also acts as a reagent ion for I₂. However,
 319 it is unlikely to act as one due to an additional collisional reaction needed for formation of Br(H₂O)₂⁻ and the likely even lower
 320 formation enthalpy between the second water cluster and a sample molecule. The second water cluster may have an indirect
 321 effect on the reduction of the increase in sensitivity. At very high humidities, the proportion of dry reagent ion continues to
 322 decrease with the first water cluster proportion remaining steady while the second water cluster increases. This suggests the
 323 formation rate of the first water cluster is being matched by its conversion to the second water cluster. This will still reduce
 324 the amount of adduct formation occurring through the more exothermic dry reagent ion pathway but will not produce an
 325 increase in sensitivity via water stabilisation. These factors potentially explain the emergence of the humidity-independent
 326 region above the 0.7 water ratio.



327

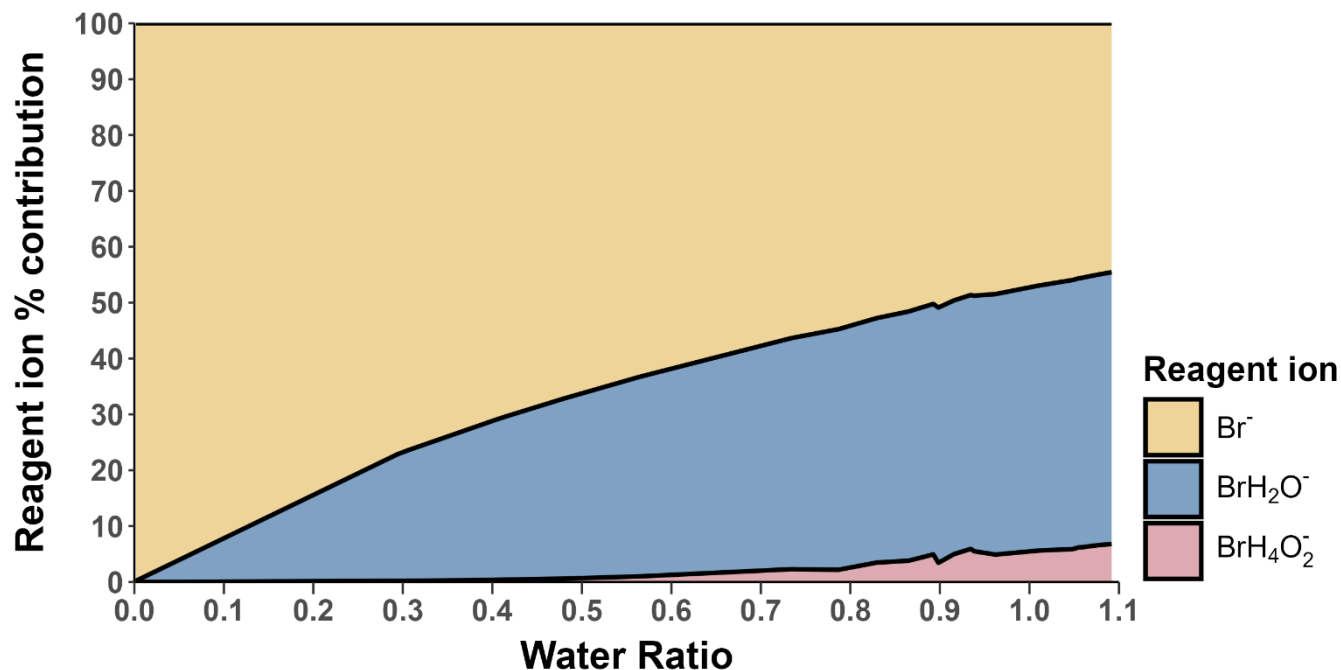
328

329

330

331

Figure 6: Measured I_2 sensitivity at different humidity levels over (a) the full range and (b) the humidity-independent range. Error bars represent the calculated error for each sensitivity value described in Sect. 3.5. The shaded grey area represents the 95% confidence interval of the fitted curve. The shaded red region represents the ambient water ratio observed in the marine boundary layer at Tudor Hill, Bermuda. The dotted line in (a) is the average of the data points in (b).



333

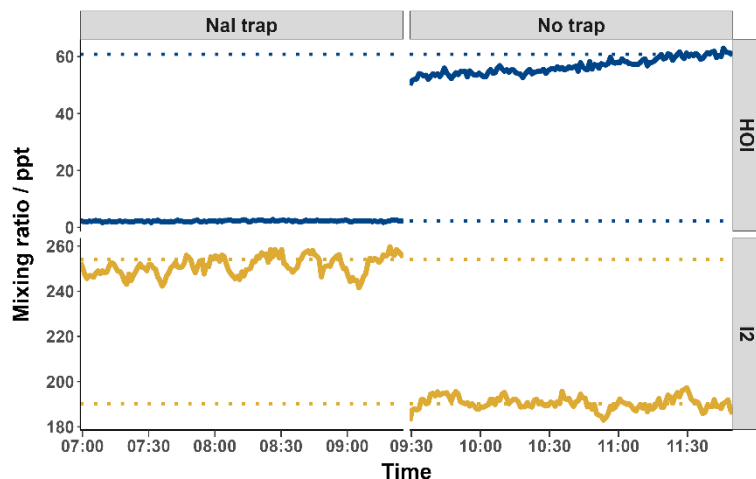
334 **Figure 7: The percentage contribution of the Br⁻ ion (yellow), BrH₂O⁻ ion (blue) and BrH₄O₂⁻ ion (pink) at different water ratios.**
 335 **The values shown are the average contributions of these ions detected during the I₂ calibration runs.**

336

337 3.4 HOI calibration and humidity dependence

338 The relative sensitivity of HOI compared to I₂ (termed the HOI/I₂ ratio) was quantified by comparing the change in signal of
 339 HOI and I₂ with and without the NaI trap in place, with an example calibration shown in Fig. 8. With no trap in place, the ratio
 340 of HOI to I₂ signal was found to be around 1:5. On addition of the NaI trap, almost all of the HOI signal was removed with a
 341 corresponding increase in I₂ signal observed. For the equivalent HOBr–Br₂ system in the Liao et al. (2012) system, the
 342 conversion of HOBr to Br₂ was assumed to be 1:1. Here, the 1:1 HOI to I₂ conversion assumption was tested by measuring the
 343 signal of various other iodine-containing compounds, to determine whether any other significant reaction pathways were
 344 occurring during the production and destruction of HOI. The mass spectra of these other iodine compounds are shown including
 345 the NaI trap in Fig. A2 and without the trap in Fig. A3. Some of these compounds have substantial overlapping interfering
 346 peaks, and it is not possible at the instrument resolution to determine how real their signals are. Of these compounds, only HI
 347 and IBr had both distinct enough peaks and showed a small increase on addition of the NaI trap. The increase in HI and IBr
 348 signals were much smaller than for I₂, which represented 96% of the change in signal, as shown in Table A1. The production
 349 of HI is likely from the reaction of NaI and HNO₃, which is produced via (R12) in the HOI generation step, rather than from
 350 HOI. It is possible that the IBr signal may be produced from HOI, for example if there was some contaminant NaBr also

351 present in the trap. Conversely, any contaminant bromine compounds in the gas stream may react with the NaI trap, producing
352 the IBr. However, the average standard error of the I₂ signal change is already higher than the increase in IBr signal, and so
353 the production of IBr can be considered negligible against the other uncertainties of the calibration and the assumed 1:1
354 conversion of HOI to I₂ can be maintained.
355

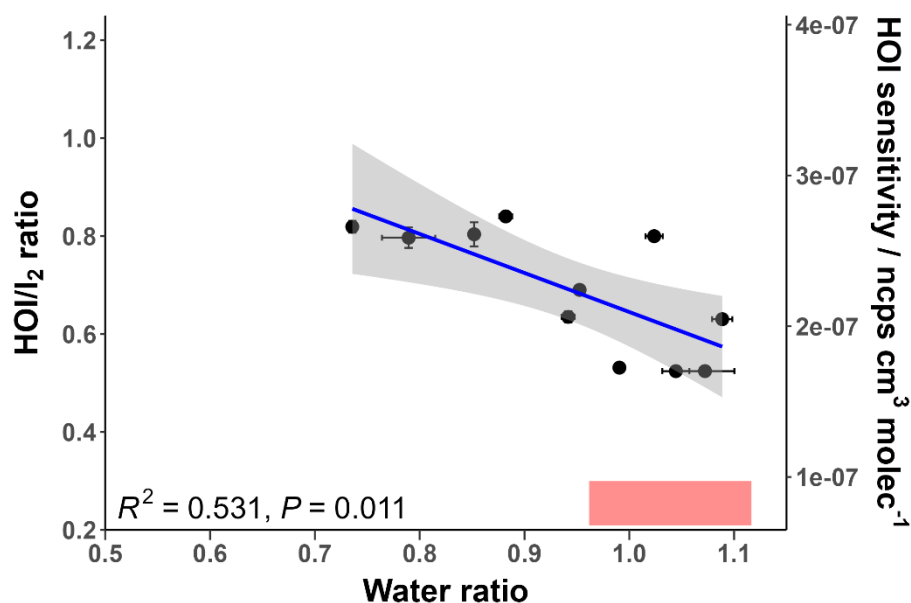


356

357 **Figure 8: 1-minute averaged HOI and I₂ mixing ratios with and without the inclusion of the NaI trap. Dotted lines indicate the**
358 **average mixing ratio of the final 20 minutes of each run. Values were calculated according to the calibration curve from Fig 9.**

359

360 The HOI calibration experiments were performed at different water ratios to determine how the HOI/I₂ ratio changes with
361 humidity. As water was required to generate HOI in the first stage of the calibration, the experiments were only able to be
362 performed at relatively high humidity, between water ratios of 0.7 and 1.1. This range corresponds to the humidity-independent
363 region found for I₂. The humidity dependence of the HOI/I₂ ratio is shown in Fig. 9.



364

365 **Figure 9: The relative sensitivity of HOI compared to I₂ (HOI/I₂ ratio) at different water ratio values. The regression line follows the**
 366 **equation $y = 1.44 - 0.798x$. The secondary y-axis shows the corresponding HOI sensitivity compared to the HOI/I₂ ratio. The shaded**
 367 **grey area represents the 95% confidence interval of the fitted regression line. The shaded red region represents the ambient water**
 368 **ratio observed in the marine boundary layer at Tudor Hill, Bermuda.**

369

370 Figure 9 shows that the HOI/I₂ ratio moderately correlates with increasing humidity; the correlation is statistically significant
 371 with a P-value below 0.05. As the humidity dependence of I₂ is independent over this measurement range, this decrease is
 372 attributed to a decreasing sensitivity for HOI. This can be explained from a QRRK theory standpoint. As seen in Table 1, the
 373 HOI.Br⁻ cluster has more accessible vibrational modes than I₂.Br⁻, so the increase in vibrational modes from the presence of
 374 water will have a smaller stabilising effect for HOI.Br⁻ than for I₂.Br⁻. Additionally, the formation enthalpy for the HOI.Br⁻
 375 cluster is lower than for I₂.Br⁻, and so the effect of reducing the amount of formation via the dry reagent ion has a more
 376 pronounced effect on the HOI.Br⁻ cluster.

377 3.5 Sensitivity measurement uncertainty

378 Propagation of error was used to calculate the uncertainty of the I₂ and HOI sensitivities. This can be calculated using the exact
 379 formula of propagation, assuming that variables are independent of each other, as shown in Eq. (4).

380

$$381 \sigma_x = \sqrt{\left(\frac{\partial x}{\partial a}\right)^2 \cdot \sigma_a^2 + \left(\frac{\partial x}{\partial b}\right)^2 \cdot \sigma_b^2 + \left(\frac{\partial x}{\partial c}\right)^2 \cdot \sigma_c^2 + \dots + \left(\frac{\partial x}{\partial n}\right)^2 \cdot \sigma_n^2} \quad (4)$$

382

383 where a, b, c, \dots, n are the variables of the function x , ∂_x/∂_n is the partial derivative of the variable with respect to x , and σ_n is
384 the error of the individual variable.

385 3.5.1 I₂

386 The I₂ concentration error was calculated from the propagation of the uncertainties of the emission of the I₂ permeation tube,
387 the temperature of the permeation tube holder, and the total gas flow from the sample pump to give a relative error of 0.7%.
388 The uncertainty of the sensitivity from a specific humidity calibration was calculated from the propagated uncertainty of the
389 I₂ concentration and the instrument signal for each point in the calibration curve, as shown in Fig. 5. The uncertainties of the
390 sensitivities in the humidity independent region can be averaged using Eq. (5) as these can be considered as repeats.

391

$$392 \sigma_{\text{humidity independent sensitivity}} = \frac{\sqrt{\sum_{i=1}^n (\sigma_i)^2}}{n} \quad (5)$$

393

394 where σ_i is the uncertainty of a particular sensitivity measurement and n is the number of measurements made in the humidity
395 independent region.

396

397 This resulted in a sensitivity uncertainty of 6.30×10^{-9} ncps cm³ molecules⁻¹ for the humidity-independent region, corresponding
398 to a relative error of 1.9%. This was repeated for the dry calibration sensitivities to produce an uncertainty of 3.18×10^{-9} ncps
399 cm³ molecules⁻¹ which represents a relative error of 4.0%. This uncertainty encompasses both calibration and humidity-
400 dependence uncertainties, but not background (zero) or inlet effects (see Sect. 3.6).

401 3.5.2 HOI

402 The sensitivity of HOI was determined relative to I₂ based on the linear model in Fig. 9. The uncertainty of the HOI sensitivity
403 at a specific water ratio was found from the uncertainty of the I₂ sensitivity at that water ratio propagated with the uncertainty
404 of the gradient and intercept of the linear model. This results in an uncertainty of 4.29×10^{-8} ncps cm³ molecules⁻¹ for the HOI
405 sensitivity, corresponding to an average relative error of 19.8% with a range of 16-25%, neglecting any background and inlet
406 effects.

407 3.6 Inlet loss considerations

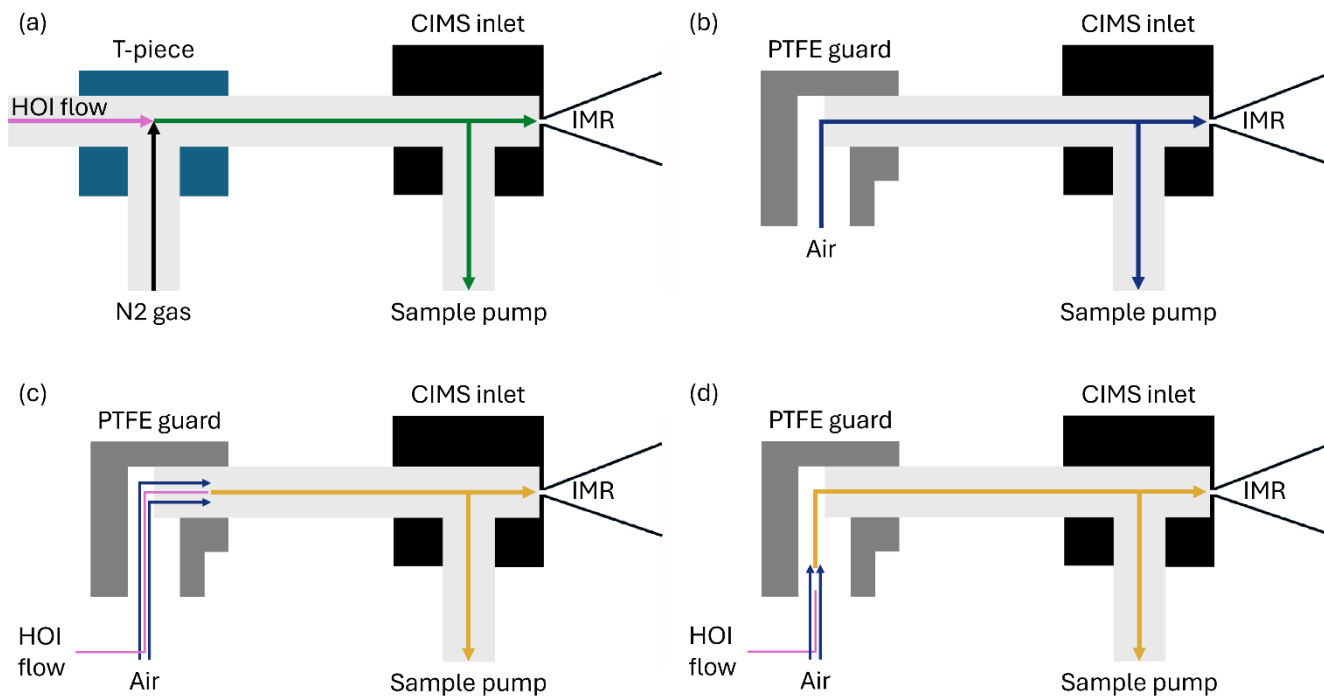
408 Measuring gas-phase compounds through an instrument inlet will introduce gas-wall interactions that can lead to loss of signal
409 or require conditioning to reach a steady state (Krechmer et al., 2016; Huang et al., 2018; Deming et al., 2019). Additionally,
410 halogen compounds can undergo heterogeneous chemistry on inlet walls, resulting in conversion to other halogen compounds.
411 This is particularly the case for the hypohalous acids and has been observed for HOBr and HOCl when measured by CIMS
412 instruments (Neuman et al., 2010; Liao et al., 2014; Le Breton et al., 2017; Peng et al., 2022). While all halogen compounds

413 experience these wall interactions, it is particularly pronounced for iodine compounds, leading to large losses and uncertainties
414 in measurements. Previous measurements of I₂ have found sample line losses between 18–40% (Shaw and Carpenter, 2013;
415 Carpenter et al., 2013). For HOI, the calibration performed by Tham et al. (2021) modelled the loss of HOI through their inlet
416 system via diffusion to the inlet walls which contributed to their total HOI uncertainty of ± 55%.

417
418 The effect of inlet losses is heavily influenced by the instrument setup. This means that any differences in inlet configuration
419 between calibrations and field measurements need to be accounted for. When deployed in the field, the inlet for this instrument
420 had a PTFE guard, allowing sample air to enter the inlet at a 90° angle, shown in Fig. 10b. The guard was implemented with
421 the intention that light gas-phase molecules could navigate around the bend without loss to the walls, but heavier aerosol
422 particles could not, reducing the potential for aerosol to block the entrance to the CIMS instrument. However, when calibrating,
423 the calibration gas was directed linearly into the sampling inlet, shown in Fig. 10a. The effect of this difference was
424 investigated.

425
426 Two inlet loss experiments were performed, one using a PFA T-piece to investigate the effect of physically having a bend in
427 place, and another with the PTFE guard that had been salted with sea water to mimic field conditions. A line of 1/8" PFA
428 tubing was attached to the output of the HOI calibration system and held in two configurations: one where it is pushed past the
429 bend as shown in Fig. 10c and one where it is held before it, Fig. 10d. This required altering the dilution flow to laboratory air
430 to accommodate this configuration. The effect of the T-piece and PTFE guard on the normalised signal of HOI and I₂, along
431 with other iodine compounds that are potentially present, are shown in Table 2.

432



433

434

435

436

Figure 10: Simplified diagrams of the CIMS inlet setup during (a) the HOI calibration experiments, (b) sampling of air at Tudor Hill in Bermuda, (c) the line loss experiment bypassing the PTFE guard bend, (d) the line loss experiment including the bend from the PTFE guard.

437
438**Table 2: The normalised signal ± 1 standard deviation of various iodine species measured during the direct and bended inlet configurations for the T-piece and PTFE guard inlet loss experiments.**

Species	T-piece			PTFE guard		
	Direct configuration $\pm 1\sigma$ / ncps	Bend configuration $\pm 1\sigma$ / ncps	Signal difference / ncps (% change)	Direct configuration $\pm 1\sigma$	Bend configuration $\pm 1\sigma$	Signal difference / ncps (% change)
HOI	381.45 \pm 5.85	132.79 \pm 6.38	-248.66 (-65%)	335.05 \pm 5.79	85.13 \pm 2.59	-249.92 (-75%)
I ₂	2576.62 \pm 25.92	2985.40 \pm 49.75	+408.78 (+16%)	2149.51 \pm 23.18	2472.60 \pm 25.23	+323.09 (+15%)
ICl	371.44 \pm 8.45	375.98 \pm 10.53	+4.54 (+1%)	400.73 \pm 8.62	531.58 \pm 15.02	+130.85 (+33%)
IBr	20.82 \pm 1.47	17.34 \pm 1.81	-3.48 (-17%)	20.32 \pm 1.51	185.06 \pm 4.57	+164.74 (+811%)
HI	0.16 \pm 0.42	0.20 \pm 0.44	+0.04 (+25%)	0.17 \pm 0.43	0.27 \pm 0.47	+0.10 (+59%)
IO	1.04 \pm 0.37	1.42 \pm 0.71	+0.38 (+37%)	1.23 \pm 0.35	1.02 \pm 0.50	-0.21 (-17%)
HIO ₂	27.67 \pm 3.77	30.36 \pm 9.74	+2.69 (+10%)	26.73 \pm 5.01	28.12 \pm 4.75	+1.39 (+5%)
INO ₂	2.30 \pm 0.73	1.00 \pm 0.58	-1.30 (-57%)	2.36 \pm 0.74	1.17 \pm 0.50	-1.19 (-50%)
HIO ₃	0.79 \pm 0.50	0.58 \pm 0.64	-0.21 (-27%)	1.02 \pm 0.56	0.93 \pm 0.63	-0.09 (-9%)
IONO ₂	6.75 \pm 1.39	2.51 \pm 1.28	-4.24 (-63%)	6.48 \pm 1.57	3.30 \pm 1.33	-3.18 (-49%)

439

440 For both the T-piece and the guard, the direct signal is comparable in intensity to the signal seen during the HOI calibrations,
441 with the exception of ICl, which is much higher than previously seen. When including the bend into the T-piece experiment,
442 little variation in signal is observed for ICl, HI, IO, HIO₂, and HIO₃, with changes smaller than the standard deviation of the
443 signal. There is a slight decrease in the IBr, INO₂, and IONO₂ signal, but the total quantity of loss from these compounds is
444 small compared to the total loss (<4%) The most noticeable loss is observed with HOI, along with an accompanying increase
445 in I₂. When converted into mixing ratios this corresponded to a 42.7 ppt (65%) HOI decrease and a 50.5 ppt (16%) increase in
446 I₂. This conversion of HOI to I₂ likely proceeds via the reverse iodine hydrolysis reaction (R14). The I⁻ required is most likely
447 from the HOI generation reaction in (R8), which becomes coated on the inlet walls. It is unknown how much I⁻ is present
448 during field measurements, and so the observed I₂ increase found during the inlet loss tests may be an overestimate compared
449 to atmospheric conditions.

450



452

453 With the salted PTFE guard, a higher proportion of HOI was lost (75% decrease) compared to the T-piece although the amount
454 lost was similar at 43.4 ppt. Meanwhile the proportion of I₂ gain remained about the same (15% increase) but the amount has
455 decreased to 40.0 ppt. There is a marked increase in IBr and ICl signal and the other iodine species remain at similar levels to
456 the T-piece run. Cl⁻ and Br⁻ are abundant in sea salt aerosol and are known to react with HOI (Vogt et al., 1999; Braban et al.,
457 2007; Tham et al., 2021), which is the likely reason for the increase in ICl and IBr and further loss of HOI compared to the T-
458 piece experiment. The sensitivities for ICl and IBr have not been measured for Br-CIMS instruments. However, it has been
459 suggested that sensitivities should be similar to that of I₂ (Wang et al., 2021a). If it is assumed that ICl and IBr have the same
460 response to humidity as I₂, the signal change would correspond to a 16.9 and 20.2 ppt increase, respectively. This is far higher
461 than would be expected from the additional HOI loss and may suggest there are additional pathways present to produce ICl
462 and IBr.

463 **3.7 Application to atmospheric HOI and I₂ data**

464 I₂ and HOI were measured by the Br-CIMS during the BLEACH campaign in June 2022 with the inlet configuration shown
465 in Fig. 10b. Background signals were measured by flowing dry nitrogen (N₂) through a zero port in the CIMS inlet and through
466 the instrument critical orifice to the IMR, with the rest of the sampled air directed through the sample pump. These zero
467 measurements were repeated hourly, and the signal was linearly interpolated between measurements, providing a value for the
468 background signal during sampling periods. The limit of detection (LoD) for I₂ and HOI were calculated from an extended
469 zeroing period during the campaign as 3 standard deviations of the Allen variance of the zeroing period, similarly to that
470 described in Riva et al. (2024). These corresponded to detection limits of 0.14 ppt for I₂ and 0.27 ppt for HOI.

471

472 The HOI calibration could not be performed at dryness, making zero subtraction difficult to quantify. The HOI/I₂ ratio from
 473 Fig. 9 could be extrapolated to dryness at the y-intercept which would result in a dry HOI sensitivity that is 1.44 times higher
 474 than I₂. However, the 95% confidence interval of the intercept is ±0.43, suggesting a low precision when extrapolating from
 475 this calibration. An alternative method is to use the quantum chemical calculations to compare the decay rate between the
 476 HOI.Br⁻ and I₂.Br⁻ clusters. Using the values from Table 1, the decay rate of HOI.Br⁻ is slightly slower than I₂.Br⁻, which would
 477 suggest a slightly higher sensitivity at dryness. However, this value is still similar to the decay rate of I₂.Br⁻, and so the dry
 478 sensitivity of I₂ could be used as a conservative estimate of the dry HOI sensitivity.

479
 480 It is also possible that any signal observed in the zero for HOI and I₂ was due to instrument noise rather than any interferent
 481 compounds. This was tested by comparing the relative signal intensities of two major isotope peaks of the I₂.Br⁻ and HOI.Br⁻
 482 adducts. The theoretical ratios between I₂.⁷⁹Br⁻ and I₂.⁸¹Br⁻ and HOI.⁷⁹Br⁻ and HOI.⁸¹Br⁻ are 1:0.975 and 1:0.977, respectively.
 483 The zero data was tested to see whether the ratio between the isotope peaks were within 10, 20 or 30% of this ratio. These
 484 values are shown in Table 3. For I₂, 72% of the zero data fell within the 30% ratio limit, suggesting that the signal is generally
 485 real and needs to be accounted for by zero subtraction. For HOI, 74% of the zero data had isotope ratios that were greater than
 486 the 30% tolerance, indicating that the signal generally may not be real. Both the sample and zero timeseries for HOI and I₂ are
 487 shown in Fig. A5. The sample timeseries, without zero subtraction, can be considered as an upper limit of the HOI and I₂
 488 mixing ratios.

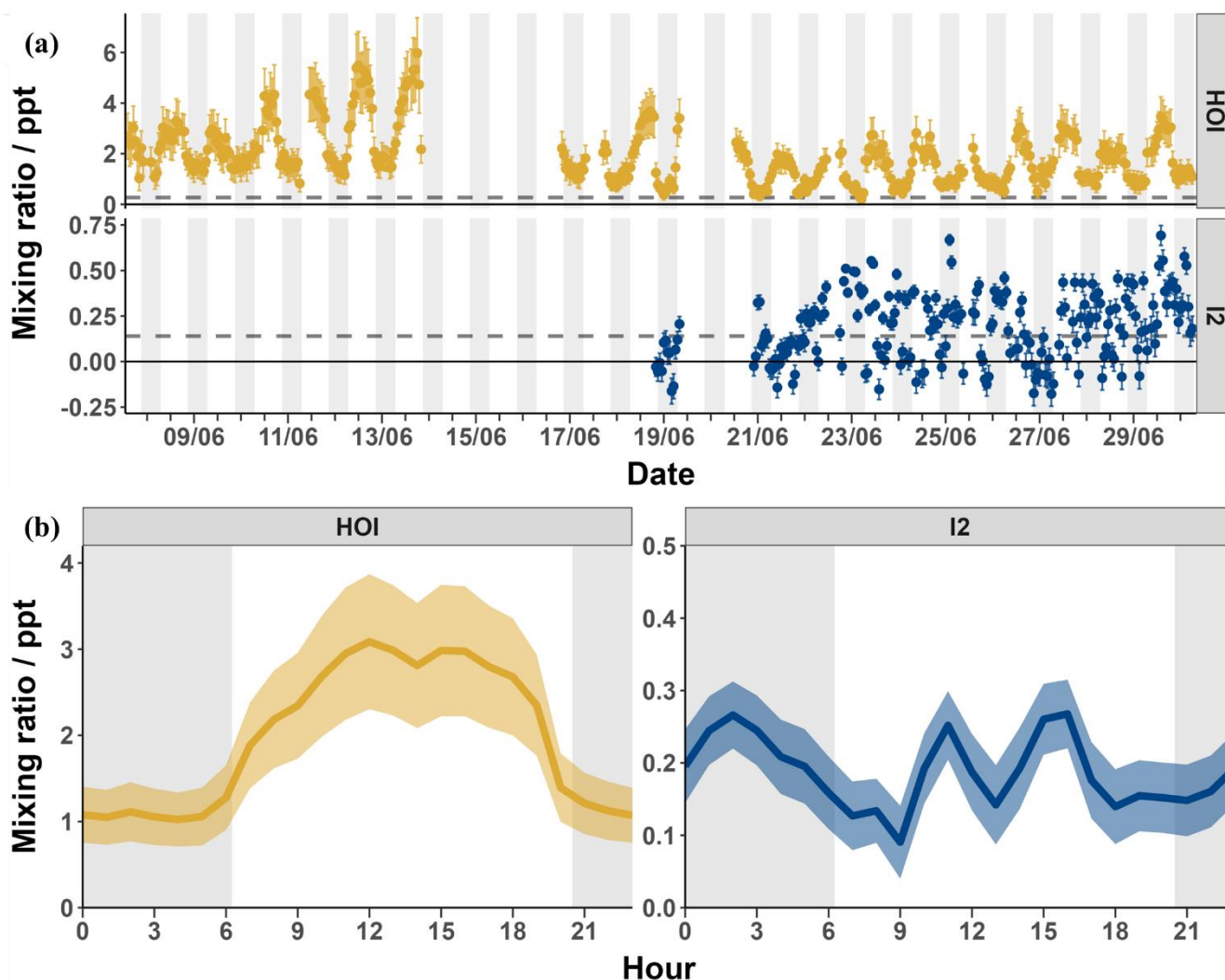
489
 490 **Table 3: The instrument zero data points during the BLEACH campaign that fell within various limits of the theoretical isotope**
 491 **ratio between the I₂.Br⁻ and HOI.Br⁻ adduct signals. A ratio value that was greater than 30% of the theoretical value was considered**
 492 **to be outside the ratio tolerance.**

	Total data points	Ratio limits			
		<10%	<20%	<30%	>30%
I ₂ zeroing data	412	129	232	297	115
	(100%)	(31.3%)	(56.3%)	(72.1%)	(27.9%)
HOI zeroing data	412	34	62	108	304
	(100%)	(8.3%)	(15.0%)	(26.2%)	(73.8%)

493
 494 Measured signals were converted into mixing ratios using the calibrations from Sect. 3.3 and 3.4 and applying the loss
 495 corrections described in Sect. 3.5. The data was then zero subtracted using the linearly interpolated instrument zeros. Figure
 496 11 shows the loss-corrected timeseries and diurnal cycles for I₂ and HOI. After zero subtractions and loss corrections, I₂ was
 497 detected between 0–0.7 ppt with some mixing ratios dropping to negative values. HOI ranged from 0.2–6.0 ppt after its zero
 498 subtractions and loss corrections. There was little pattern in the diurnal cycle for I₂ with the average signal being between 0.1–
 499 0.3 ppt during both the day and night. The observed mixing ratios of I₂ are similar to previous open ocean measurements at

500 the Cape Verde Atmospheric Observatory of <0.02 – 0.6 and <0.03 – 1.67 ppt in May 2007 and 2009 respectively (Lawler et al.,
501 2014). These previous measurements observed a diurnal cycle for I_2 peaking at night, as expected due to its rapid photolysis.
502 A diurnal cycle was not observed in our data, indicating either inlet or background effects which were not adequately quantified
503 by our experiments or an unknown or poorly quantified daytime source of I_2 . Potential daytime sources include heterogeneous
504 reactions of photochemically produced oxidants such as HOI with iodide on the surface of aerosols (Vogt et al., 1999; Moon
505 et al., 2026) or on the sea surface (Pound et al., 2024), photochemical oxidation of iodide (Raso et al., 2017) or photochemical
506 reduction of iodate (Reza et al., 2024). However, these would have to be occurring close to the measurement site due to the
507 fast photolytic lifetime of I_2 . Additionally, the release of I_2 from aerosol is also a likely contributor to the inlet effects, due to
508 buildup of aerosol on the inlet. With the inlet setup used in this work, these processes are indistinguishable. The overall
509 uncertainty of the I_2 measurements made during the BLEACH campaign, as seen in Sect. 3.7.1, and the fact that they were
510 near to the detection limit of 0.14 ppt means that caution should be applied in interpreting the data.

511
512 In contrast, a regular diurnal pattern was observed for HOI, with the signal consistently around 1 ppt during the night and
513 increasing during the day to an average peak of around 3 ppt. There are no reported mixing ratios of HOI in the open ocean to
514 compare to these values. The closest comparison is to the measurement of HOI at the coastal site of Mace Head (Tham et al.,
515 2021). There, a diurnal cycle was also observed, with low nighttime mixing ratios and an increase during the day. However,
516 the amounts seen at Mace Head during the day were much higher (up to 66.6 ppt), likely due to photochemical reactions caused
517 by I_2 emission by macroalgae (Tham et al., 2021).



518

519 **Figure 11: The timeseries (a) and diurnal cycle (b) of the mixing ratios of I₂ (blue) and HOI (yellow) from the BLEACH campaign**
 520 **in June 2022 after zero subtraction and loss correction. The dashed line indicates the limit of detection for each compound. The**
 521 **average relative uncertainty of I₂ was ± 28.7% and for HOI was ± 27.7%.**

522 3.7.1 Measurement uncertainties of atmospheric data

523 The uncertainty of the I₂ and HOI mixing ratios were again calculated by propagation of uncertainty. This was calculated from
 524 the uncertainty of the humidity independent sensitivity, twice the uncertainty of the dry sensitivity from the linear interpolation
 525 calculation, and the uncertainty of the instrument signal during the inlet loss experiment. This resulted in an average relative
 526 error throughout the BLEACH campaign of 28.7% for I₂ and 27.7% for HOI. There are a number of other uncertainties from
 527 the inlet loss experiment that cannot be quantified and so the uncertainty for I₂ and HOI should be considered a lower limit. In
 528 future work, repeated experiments may be able to account for these uncertainties by finding a standard deviation of the loss
 529 correction value.

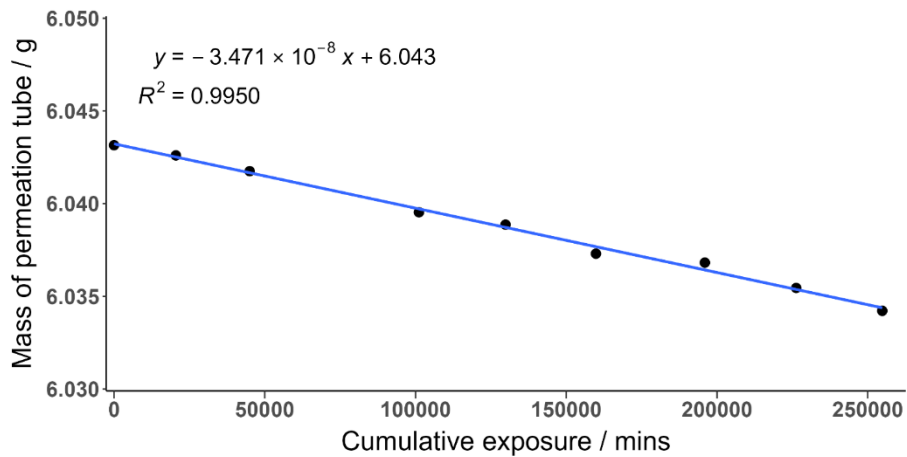
530 4. Summary and conclusions

531 There have been few atmospheric measurements of HOI and I₂ due to the requirement of highly sensitive and selective
532 instrumentation and the lack of readily available calibration methods for HOI. In this study, we demonstrate a novel method
533 for the generation and calibration of HOI at ppt levels, utilising its interconversion to I₂ via chemical traps. The presence of
534 potential interferent iodine compounds was found to be negligible and the calibration was shown to be repeatable over a range
535 of humidities. The developed calibration method was utilised to ascertain the humidity dependence of the CIMS for HOI and
536 I₂. It was found that at humidities typical of the marine boundary layer, I₂ exhibited a humidity-independent sensitivity whereas
537 HOI showed a slight negative dependency. A possible explanation, supported by QRRK theory, is that higher humidities
538 increase the proportion of the Br(H₂O)⁻ reagent ion, which has a lower adduct formation enthalpy with HOI and I₂ compared
539 to the Br⁻ reagent ion, resulting in decreased sensitivities. However, the presence of H₂O increases the available vibrational
540 modes of the adduct, improving the energy distribution and stabilisation of the adduct and increasing its sensitivity. This effect
541 is greater for I₂.Br⁻ as it has fewer harmonic oscillators than HOI.Br⁻ and these two opposing factors mean that the sensitivity
542 of I₂.Br⁻ is humidity independent. However, this stabilisation is not sufficient in the case of the HOI.Br⁻ adduct to mitigate the
543 increasing proportion of Br(H₂O)⁻ vs Br⁻ reagent ions, resulting in a decreased sensitivity at high humidities.

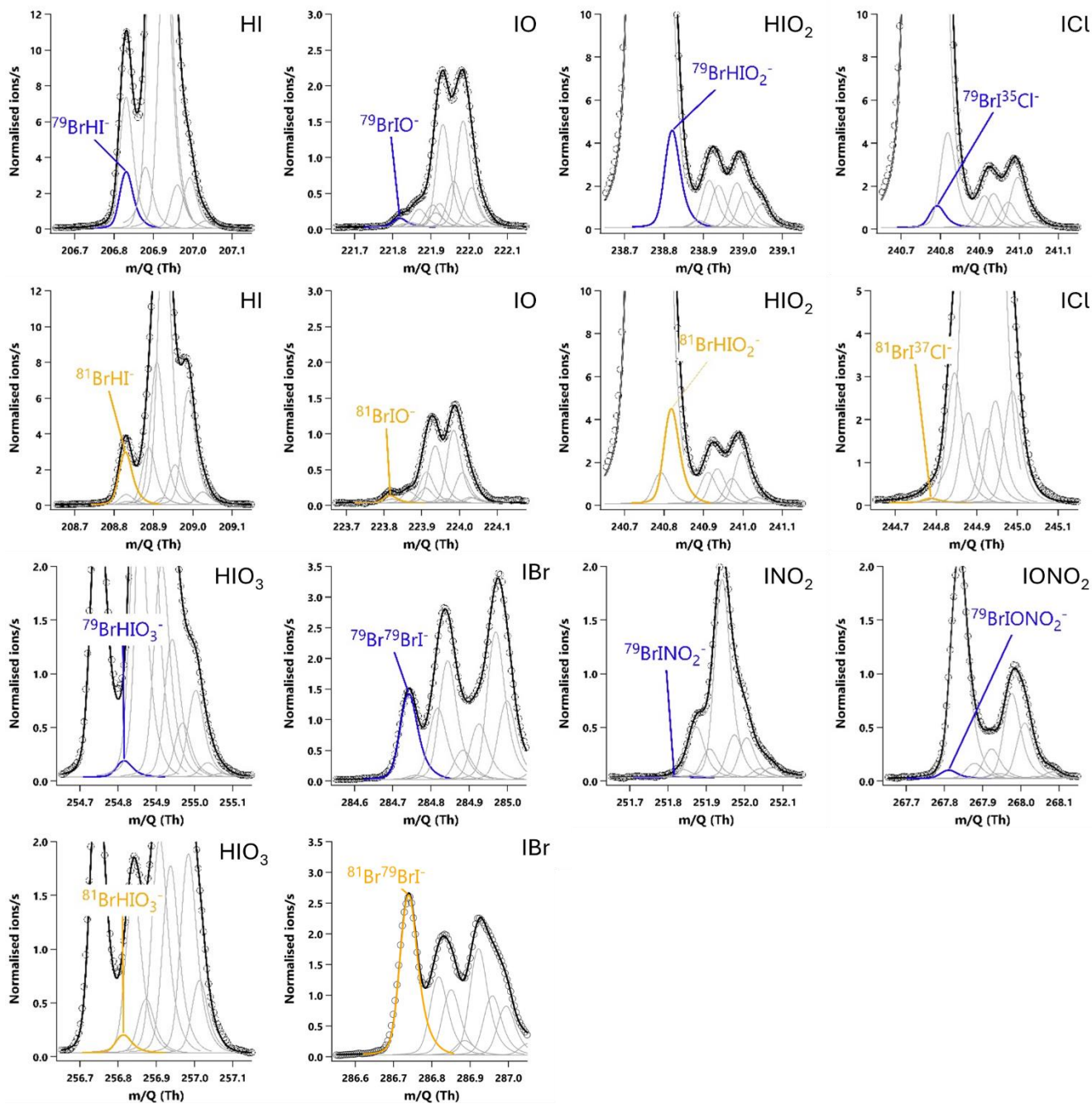
544
545 Heterogeneous chemistry and inlet wall losses are a perennial problem in the measurement of acidic and reactive species,
546 which can be exacerbated depending on the inlet configuration. When using the inlet configuration made for field
547 measurements, up to 75% of the HOI signal was lost compared to the calibration setup. This was accompanied by a
548 corresponding increase in I₂ signal, suggesting that this loss occurred via the reverse hydrolysis of iodine.

549
550 After correcting for humidity sensitivities and inlet losses, we detected I₂ and HOI in the marine boundary layer during the
551 BLEACH campaign at Tudor Hill, Bermuda in June 2022 at mixing ratios of between 0–0.7 ppt for I₂ and 0.2–6.0 ppt for HOI.
552 The overall uncertainty of these measurements was calculated as ± 28.7% for I₂ and ± 27.7% for HOI. These uncertainties can
553 be considered as lower limits as there were additional uncertainties from the inlet loss experiment that were not quantifiable.

554
555 In future work, the accuracy for I₂ and HOI could be improved by performing background measurements at similar humidity
556 levels to the ambient measurements, reducing the need to account for large differences in sensitivities from different humidities.
557 Additionally, further work on the HOI calibration can further constrain the uncertainty of the humidity dependent HOI/I₂ ratio
558 over a wider range of humidities. Finally, development of atmospheric detection of HOI and I₂ should focus on using
559 instrument inlets that can minimise inlet effects for these compounds, reducing the need to perform correction tests. Any
560 correction tests that are performed should be done before, during, and after field measurement collection to best characterise
561 any inlet artifacts and changes during the measurements.

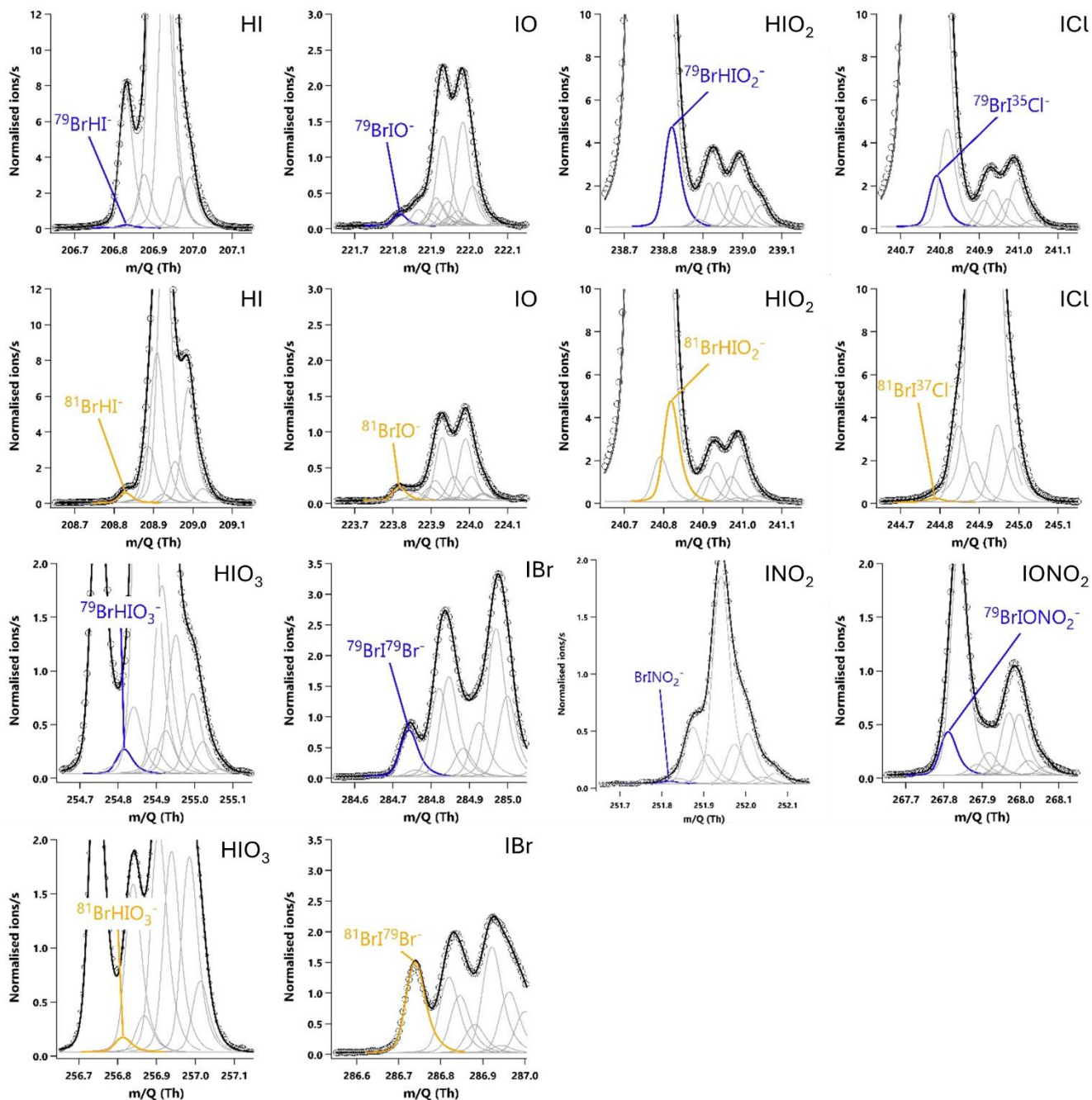


565 **Figure A1: The mass loss of an I₂ permeation tube over time. The gradient represents the emission rate of the permeation tube. Each**
566 **data point is the average of 6 measurements.**



570

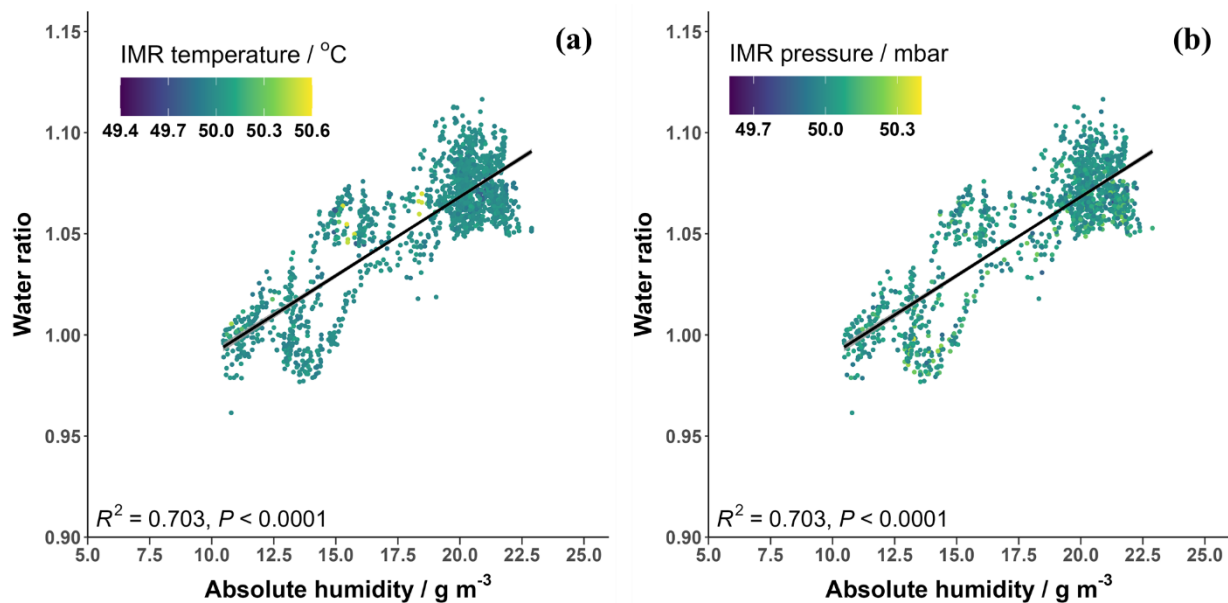
571 **Figure A2: 20-minute averaged high resolution single peak mass spectra fits for potential iodine containing compounds during the**
 572 **HOI calibrations with the NaI trap in place. The molecular ion peak is shown in blue with the primary isotope peak in gold with an**
 573 **exception for $^{81}\text{Br}^{37}\text{Cl}^-$ as this was the isotope used to calculate the BrCl signal. Isotope peak shapes were determined using the**
 574 **Tofware software. The isotope peaks of BrINO_2^- and BrIONO_2^- were not able to be visualised by the software.**



575

576 **Figure A3: 20-minute averaged high resolution single peak mass spectra fits for potential iodine containing compounds during the**
 577 **HOI calibrations after the removal of the NaI trap. The molecular ion peak is shown in blue with the primary isotope peak in gold**
 578 **with an exception for $^{81}\text{Br}^{37}\text{Cl}^-$ as this was the isotope used to calculate the BrICI signal. Isotope peak shapes were determined using**
 579 **the Tofware software. The isotope peaks of BrINO_2^- and BrIONO_2^- were not able to be visualised by the software.**

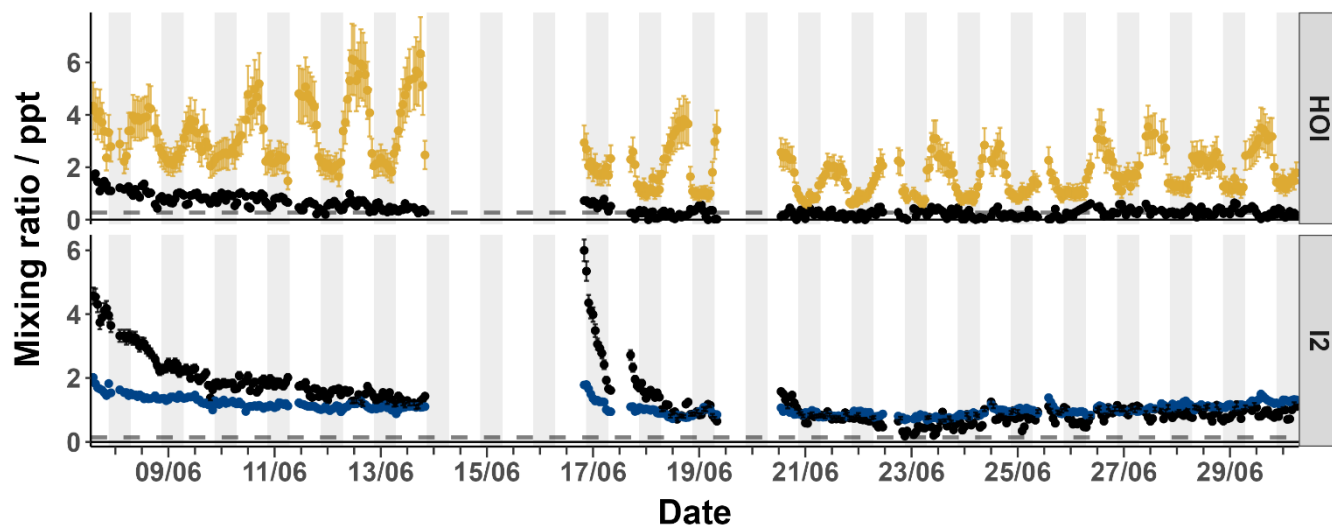
580



581

582 Figure A4: The water ratio in the CIMS IMR plotted against the absolute humidity measured during the BLEACH campaign
 583 coloured by (a) the variation in IMR temperature and (b) the variation in IMR pressure.

584



585

586 Figure A5: The timeseries of the sample mixing ratios of HOI (yellow) and I₂ (blue) along with their corresponding zero mixing
 587 ratios (black) from the BLEACH campaign in June 2022. The dashed line indicates the limit of detection for each compound.

588

589

590
591**Table A1: The signal change (in normalised ion counts per second) of HNO₃, HI, IBr and I₂ along with their calculated standard errors during the HOI calibration runs upon addition of the NaI trap.**

Run number	Signal change (\pm standard error) on addition of NaI trap / ncps			
	HNO ₃	HI	IBr	I ₂
1	-4902.1 (\pm 71.5)	36.49 (\pm 0.93)	6.84 (\pm 0.51)	430.04 (\pm 10.89)
2	-5274.0 (\pm 164.4)	20.25 (\pm 0.80)	5.07 (\pm 0.46)	451.62 (\pm 13.60)
3	-4543.7 (\pm 43.7)	11.96 (\pm 0.69)	4.73 (\pm 0.40)	519.53 (\pm 5.76)
4	-4129.3 (\pm 58.4)	10.72 (\pm 1.02)	5.82 (\pm 0.49)	573.95 (\pm 6.90)
5	-4051.3 (\pm 116.0)	13.98 (\pm 1.41)	7.24 (\pm 0.51)	517.84 (\pm 8.79)
6	-4865.5 (\pm 48.7)	6.77 (\pm 0.95)	6.98 (\pm 0.53)	662.69 (\pm 9.09)
7	-2812.2 (\pm 43.3)	6.57 (\pm 0.82)	10.66 (\pm 0.52)	424.65 (\pm 6.39)
8	-3742.2 (\pm 64.4)	24.76 (\pm 1.09)	6.89 (\pm 0.49)	391.72 (\pm 5.24)
9	-2413.3 (\pm 63.5)	6.67 (\pm 0.55)	11.63 (\pm 0.55)	553.02 (\pm 7.72)
10	-4725.2 (\pm 50.5)	4.26 (\pm 0.82)	7.35 (\pm 0.40)	516.05 (\pm 4.749)
11	-4555.5 (\pm 52.7)	2.27 (\pm 0.48)	8.04 (\pm 0.40)	884.80 (\pm 7.62)

592

593 **Data availability**

594 Datasets for the figures shown are available at: <https://doi.org/10.15124/48ade8f3-d750-4fe6-a2d9-b8f69bf86262>

595 **Author contribution**

596 LM, MS, LJC and SJA designed and developed the humidity dependence calibrations for I₂ which were conducted by LM.
597 MS, PR and JT developed the HOI calibration method and was adapted and conducted in lab experiments by LM and MZ.
598 BA was responsible for the management and coordination of the BLEACH field campaign and AP was responsible for the
599 management and usage of the Tudor Hill Marine Atmospheric Observatory.
600 PBK performed the quantum chemical calculations.
601 LM and LJC prepared the paper, and all authors reviewed the paper.

602 **Competing interests**

603 The authors declare that they have no conflict of interest.

604 **Acknowledgements**

605 The authors would like to thank John Halfacre, William Drysdale, Allison Moon, Alyson Fritzmann and Gordon Novak for
606 their help during the BLEACH summer campaign.

607 **Financial support**

608 This research was supported by the European Research Council, Horizon Europe European Research Council (grant no.
609 833290).
610 BA, JT and PR were supported by NSF AGS 2109323
611 The Tudor Hill Marine Atmospheric Observatory was supported by the National Science Foundation's Chemical
612 Oceanography Program, grant OCE-2123053.

614

- 615 Auzmendi-Murua, I., Castillo, A., and Bozzelli, J.: Mercury Oxidation via Chlorine, Bromine, and Iodine under Atmospheric
616 Conditions: Thermochemistry and Kinetics, *JOURNAL OF PHYSICAL CHEMISTRY A*, 118, 2959-2975,
617 10.1021/jp412654s, 2014.
- 618 Bitter, M., Ball, S., Povey, I., and Jones, R.: A broadband cavity ringdown spectrometer for in-situ measurements of
619 atmospheric trace gases, *ATMOSPHERIC CHEMISTRY AND PHYSICS*, 5, 2547-2560, 2005.
- 620 Breitenlechner, M., Novak, G., Neuman, J., Rollins, A., and Veres, P.: A versatile vacuum ultraviolet ion source for reduced
621 pressure bipolar chemical ionization mass spectrometry, *ATMOSPHERIC MEASUREMENT TECHNIQUES*, 15, 1159-1169,
622 10.5194/amt-15-1159-2022, 2022.
- 623 Buys, Z., Brough, N., Huey, L., Tanner, D., von Glasow, R., and Jones, A.: High temporal resolution Br₂, BrCl and BrO
624 observations in coastal Antarctica, *ATMOSPHERIC CHEMISTRY AND PHYSICS*, 13, 1329-1343, 10.5194/acp-13-1329-
625 2013, 2013.
- 626 Calvert, J. G. and Lindberg, S. E.: The potential influence of iodine-containing compounds on the chemistry of the troposphere
627 in the polar spring. II. Mercury depletion, *Atmospheric Environment*, 38, 5105-5116, 10.1016/j.atmosenv.2004.05.050, 2004.
- 628 Caram, C., Szopa, S., Cozic, A., Bekki, S., Cuevas, C., and Saiz-Lopez, A.: Sensitivity of tropospheric ozone to halogen
629 chemistry in the chemistry-climate model LMDZ-INCA vNMHC, *GEOSCIENTIFIC MODEL DEVELOPMENT*, 16, 4041-
630 4062, 10.5194/gmd-16-4041-2023, 2023.
- 631 Carpenter, L. J., MacDonald, S. M., Shaw, M. D., Kumar, R., Saunders, R. W., Parthipan, R., Wilson, J., and Plane, J. M. C.:
632 Atmospheric iodine levels influenced by sea surface emissions of inorganic iodine, *Nature Geoscience*, 6, 108-111,
633 10.1038/ngeo1687, 2013.
- 634 Chameides, W. L. and Davis, D. D.: IODINE - ITS POSSIBLE ROLE IN TROPOSPHERIC PHOTOCHEMISTRY, *Journal*
635 *of Geophysical Research-Oceans*, 85, 7383-7398, 10.1029/JC085iC12p07383, 1980.
- 636 Cuevas, C. A., Maffezzoli, N., Corella, J. P., Spolaor, A., Vallelonga, P., Kjaer, H. A., Simonsen, M., Winstrup, M., Vinther,
637 B., Horvat, C., Fernandez, R. P., Kinnison, D., Lamarque, J. F., Barbante, C., and Saiz-Lopez, A.: Rapid increase in
638 atmospheric iodine levels in the North Atlantic since the mid-20th century, *Nature Communications*, 9, 6, 10.1038/s41467-
639 018-03756-1, 2018.
- 640 Custard, K., Pratt, K., Wang, S., and Shepson, P.: Constraints on Arctic Atmospheric Chlorine Production through
641 Measurements and Simulations of Cl₂ and ClO, *ENVIRONMENTAL SCIENCE & TECHNOLOGY*, 50, 12394-
642 12400, 10.1021/acs.est.6b03909, 2016.
- 643 Deming, B., Pagonis, D., Liu, X., Day, D., Talukdar, R., Krechmer, J., de Gouw, J., Jimenez, J., and Ziemann, P.:
644 Measurements of delays of gas-phase compounds in a wide variety of tubing materials due to gas-wall interactions,
645 *ATMOSPHERIC MEASUREMENT TECHNIQUES*, 12, 3453-3461, 10.5194/amt-12-3453-2019, 2019.
- 646 Dörich, R., Eger, P., Lelieveld, J., and Crowley, J.: Iodide CIMS and m/z 62: the detection of HNO₃ as NO₃- in the presence
647 of PAN, peroxyacetic acid and ozone, *ATMOSPHERIC MEASUREMENT TECHNIQUES*, 14, 5319-5332, 10.5194/amt-14-
648 5319-2021, 2021.
- 649 Finkenzeller, H., Iyer, S., He, X., Simon, M., Koenig, T., Lee, C., Valiev, R., Hofbauer, V., Amorim, A., Baalbaki, R.,
650 Baccarini, A., Beck, L., Bell, D., Caudillo, L., Chen, D., Chiu, R., Chu, B., Dada, L., Duplissy, J., ..., and Volkamer, R.: The
651 gas-phase formation mechanism of iodic acid as an atmospheric aerosol source, *NATURE CHEMISTRY*, 15, 129-+,
652 10.1038/s41557-022-01067-z, 2023.
- 653 Frisch, M. J., Trucks, G. W., Schlegel, H. B., Scuseria, G. E., Robb, M. A., Cheeseman, J. R., Scalmani, G., Barone, V.,
654 Petersson, G. A., Nakatsuji, H., Li, X., Caricato, M., Marenich, A. V., Bloino, J., Janesko, B. G., Gomperts, R., Mennucci, B.,
655 Hratchian, H. P., Ortiz, J. V., ..., and Fox, D. J.: Gaussian 16 Rev. C.02 [code], 2019.
- 656 Garland, J. A., Elzerman, A. W., and Penkett, S. A.: THE MECHANISM FOR DRY DEPOSITION OF OZONE TO
657 SEAWATER SURFACES, *Journal of Geophysical Research-Oceans*, 85, 7488-7492, 10.1029/JC085iC12p07488, 1980.
- 658 He, X., Shen, J., Iyer, S., Juuti, P., Zhang, J., Koirala, M., Kytökari, M., Worsnop, D., Rissanen, M., Kulmala, M., Maier, N.,
659 Mikkilä, J., Sipilä, M., and Kangasluoma, J.: Characterisation of gaseous iodine species detection using the multi-scheme

660 chemical ionisation inlet 2 with bromide and nitrate chemical ionisation methods, *ATMOSPHERIC MEASUREMENT*
661 *TECHNIQUES*, 16, 4461-4487, 10.5194/amt-16-4461-2023, 2023.

662 Huang, R., Seitz, K., Buxmann, J., Pöhler, D., Hornsby, K., Carpenter, L., Platt, U., and Hoffmann, T.: In situ measurements
663 of molecular iodine in the marine boundary layer: the link to macroalgae and the implications for O₃, IO, OIO
664 and NO_x, *ATMOSPHERIC CHEMISTRY AND PHYSICS*, 10, 4823-4833, 10.5194/acp-10-4823-2010, 2010.

665 Huang, Y., Zhao, R., Charan, S., Kenseth, C., Zhang, X., and Seinfeld, J.: Unified Theory of Vapor-Wall Mass Transport in
666 Teflon-Walled Environmental Chambers, *ENVIRONMENTAL SCIENCE & TECHNOLOGY*, 52, 2134-2142,
667 10.1021/acs.est.7b05575, 2018.

668 Huey, L.: Measurement of trace atmospheric species by chemical ionization mass spectrometry: Speciation of reactive nitrogen
669 and future directions, *MASS SPECTROMETRY REVIEWS*, 26, 166-184, 10.1002/mas.20118, 2007.

670 Iglesias-Suarez, F., Badia, A., Fernandez, R. P., Cuevas, C. A., Kinnison, D. E., Tilmes, S., Lamarque, J. F., Long, M. C.,
671 Hossaini, R., and Saiz-Lopez, A.: Natural halogens buffer tropospheric ozone in a changing climate, *Nature Climate Change*,
672 10, 147-+, 10.1038/s41558-019-0675-6, 2020.

673 Iyer, S., Lopez-Hilfiker, F., Lee, B., Thornton, J., and Kurtén, T.: Modeling the Detection of Organic and Inorganic Compounds
674 Using Iodide-Based Chemical Ionization, *JOURNAL OF PHYSICAL CHEMISTRY A*, 120, 576-587,
675 10.1021/acs.jpca.5b09837, 2016.

676 Ji, Y., Huey, G., Tanner, D. J., Lee, Y. R., Veres, P. R., Neuman, J. A., Wang, Y. H., and Wang, X. M.: A vacuum ultraviolet
677 ion source (VUV-IS) for iodide-chemical ionization mass spectrometry: a substitute for radioactive ion sources, *Atmospheric*
678 *Measurement Techniques*, 13, 3683-3696, 10.5194/amt-13-3683-2020, 2020.

679 Kassel, L. S.: Studies in homogeneous gas reactions II Introduction of quantum theory, *Journal of Physical Chemistry*, 32,
680 1065-1079, 10.1021/j150289a011, 1928.

681 Kercher, J. P., Riedel, T. P., and Thornton, J. A.: Chlorine activation by N₂O₅: simultaneous, in
682 situ detection of ClNO₂ and N₂O₅ by chemical ionization mass spectrometry,
683 *Atmospheric Measurement Techniques*, 2, 193-204, 10.5194/amt-2-193-2009, 2009.

684 Klobas, J., Hansen, J., Weisenstein, D., Kennedy, R., and Wilmouth, D.: Sensitivity of Iodine-Mediated Stratospheric Ozone
685 Loss Chemistry to Future Chemistry-Climate Scenarios, *FRONTIERS IN EARTH SCIENCE*, 9, 10.3389/feart.2021.617586,
686 2021.

687 Koenig, T., Baidar, S., Campuzano-Jost, P., Cuevas, C., Dix, B., Fernandez, R., Guo, H., Hall, S., Kinnison, D., Nault, B.,
688 Ullmann, K., Jimenez, J., Saiz-Lopez, A., and Volkamer, R.: Quantitative detection of iodine in the stratosphere,
689 *PROCEEDINGS OF THE NATIONAL ACADEMY OF SCIENCES OF THE UNITED STATES OF AMERICA*, 117, 1860-
690 1866, 10.1073/pnas.1916828117, 2020.

691 Krechmer, J., Pagonis, D., Ziemann, P., and Jimenez, J.: Quantification of Gas-Wall Partitioning in Teflon Environmental
692 Chambers Using Rapid Bursts of Low-Volatility Oxidized Species Generated in Situ, *ENVIRONMENTAL SCIENCE &*
693 *TECHNOLOGY*, 50, 5757-5765, 10.1021/acs.est.6b00606, 2016.

694 Kurtén, T., Kuang, C. A., Gómez, P., McMurry, P. H., Vehkamäki, H., Ortega, I., Noppel, M., and Kulmala, M.: The role of
695 cluster energy nonaccommodation in atmospheric sulfuric acid nucleation, *Journal of Chemical Physics*, 132, 8,
696 10.1063/1.3291213, 2010.

697 Laidler, K.: *Chemical Kinetics*, 3rd, Harper & Row, 531 pp.1987.

698 Lawler, M., Mahajan, A., Saiz-Lopez, A., and Saltzman, E.: Observations of I₂ at a remote marine site,
699 *ATMOSPHERIC CHEMISTRY AND PHYSICS*, 14, 2669-2678, 10.5194/acp-14-2669-2014, 2014.

700 Lawler, M. J., Sander, R., Carpenter, L. J., Lee, J. D., Von Glasow, R., Sommariva, R., and Saltzman, E. S.: HOCl and
701 Cl₂ observations in marine air, *Atmospheric Chemistry and Physics*, 11, 7617-7628, 10.5194/acp-11-7617-2011,
702 2011.

703 Le Breton, M., Bannan, T., Shallcross, D., Khan, M., Evans, M., Lee, J., Lidster, R., Andrews, S., Carpenter, L., Schmidt, J.,
704 Jacob, D., Harris, N., Bauguutte, S., Gallagher, M., Bacak, A., Leather, K., and Percival, C.: Enhanced ozone loss by active
705 inorganic bromine chemistry in the tropical troposphere, *ATMOSPHERIC ENVIRONMENT*, 155, 21-28,
706 10.1016/j.atmosenv.2017.02.003, 2017.

707 Lee, B., Lopez-Hilfiker, F., Veres, P., McDuffie, E., Fibiger, D., Sparks, T., Ebben, C., Green, J., Schroder, J., Campuzano-
708 Jost, P., Iyer, S., D'Ambro, E., Schobesberger, S., Brown, S., Wooldridge, P., Cohen, R., Fiddler, M., Bililign, S., Jimenez, J.,
709 ..., and Thornton, J.: Flight Deployment of a High-Resolution Time-of-Flight Chemical Ionization Mass Spectrometer:

710 Observations of Reactive Halogen and Nitrogen Oxide Species, *JOURNAL OF GEOPHYSICAL RESEARCH-*
711 *ATMOSPHERES*, 123, 7670-7686, 10.1029/2017JD028082, 2018.

712 Lee, B. H., Lopez-Hilfiker, F. D., Mohr, C., Kurtén, T., Worsnop, D. R., and Thornton, J. A.: An Iodide-Adduct High-
713 Resolution Time-of-Flight Chemical-Ionization Mass Spectrometer: Application to Atmospheric Inorganic and Organic
714 Compounds, *Environmental Science & Technology*, 48, 6309-6317, 10.1021/es500362a, 2014.

715 Lee, C., Elgiar, T., David, L., Wilmot, T., Reza, M., Hirshorn, N., McCubbin, I., Shah, V., Lin, J., Lyman, S., Hallar, A., Gratz,
716 L., and Volkamer, R.: Elevated Tropospheric Iodine Over the Central Continental United States: Is Iodine a Major Oxidant of
717 Atmospheric Mercury?, *GEOPHYSICAL RESEARCH LETTERS*, 51, 10.1029/2024GL109247, 2024.

718 Legrand, M., McConnell, J., Preunkert, S., Arienzo, M., Chellman, N., Gleason, K., Sherwen, T., Evans, M., and Carpenter,
719 L.: Alpine ice evidence of a three-fold increase in atmospheric iodine deposition since 1950 in Europe due to increasing oceanic
720 emissions, *PROCEEDINGS OF THE NATIONAL ACADEMY OF SCIENCES OF THE UNITED STATES OF AMERICA*,
721 115, 12136-12141, 10.1073/pnas.1809867115, 2018.

722 Liao, J., Huey, L., Liu, Z., Tanner, D., Cantrell, C., Orlando, J., Flocke, F., Shepson, P., Weinheimer, A., Hall, S., Ullmann,
723 K., Beine, H., Wang, Y., Ingall, E., Stephens, C., Hornbrook, R., Apel, E., Riemer, D., Fried, A., ..., and Nowak, J.: High levels
724 of molecular chlorine in the Arctic atmosphere, *NATURE GEOSCIENCE*, 7, 91-94, 10.1038/NGEO2046, 2014.

725 Liao, J., Huey, L. G., Scheuer, E., Dibb, J. E., Stickel, R. E., Tanner, D. J., Neuman, J. A., Nowak, J. B., Choi, S., Wang, Y.,
726 Salawitch, R. J., Canty, T., Chance, K., Kurosu, T., Suleiman, R., Weinheimer, A. J., Shetter, R. E., Fried, A., Brune, W., ...,
727 and Ingall, E. D.: Characterization of soluble bromide measurements and a case study of BrO observations during ARCTAS,
728 *Atmospheric Chemistry and Physics*, 12, 1327-1338, 10.5194/acp-12-1327-2012, 2012.

729 MacDonald, S., Martín, J., Chance, R., Warriner, S., Saiz-Lopez, A., Carpenter, L., and Plane, J.: A laboratory characterisation
730 of inorganic iodine emissions from the sea surface: dependence on oceanic variables and parameterisation for global modelling,
731 *ATMOSPHERIC CHEMISTRY AND PHYSICS*, 14, 5841-5852, 10.5194/acp-14-5841-2014, 2014.

732 Mahajan, A., Oetjen, H., Saiz-Lopez, A., Lee, J., McFiggans, G., and Plane, J.: Reactive iodine species in a semi-polluted
733 environment, *GEOPHYSICAL RESEARCH LETTERS*, 36, 10.1029/2009GL038018, 2009.

734 Marcy, T., Gao, R., Northway, M., Popp, P., Stark, H., and Fahey, D.: Using chemical ionization mass spectrometry for
735 detection of HNO₃, HOI, and ClONO₂ in the atmosphere, *INTERNATIONAL JOURNAL OF MASS SPECTROMETRY*,
736 243, 63-70, 10.1016/j.ijms.2004.11.012, 2005.

737 Moon, A., Liu, L., Wang, X., Chan, Y., Fritzmann, A., Pound, R., Lees, A., Marden, L., Evans, M., Carpenter, L., Stutz, J.,
738 Thornton, J., Novak, G., Rollins, A., Schill, G., He, X., Finkenzeller, H., Reza, M., Volkamer, R., ..., and Alexander, B.:
739 Aerosol iodine recycling is a major control on tropospheric reactive iodine abundance, *ATMOSPHERIC CHEMISTRY AND*
740 *PHYSICS*, 26, 2353-2389, 10.5194/acp-26-2353-2026, 2026.

741 Neale, P., Hylander, S., Banaszak, A., Häder, D., Rose, K., Vione, D., Wängberg, S., Jansen, M., Busquets, R., Andersen, M.,
742 Madronich, S., Hanson, M., Schikowski, T., Solomon, K., Sulzberger, B., Wallington, T., Heikkilä, A., Pandey, K., Andradý,
743 A., ..., and Zepp, R.: Environmental consequences of interacting effects of changes in stratospheric ozone, ultraviolet radiation,
744 and climate: UNEP Environmental Effects Assessment Panel, Update 2024, *PHOTOCHEMICAL & PHOTOBIOLOGICAL*
745 *SCIENCES*, 24, 357-392, 10.1007/s43630-025-00687-x, 2025.

746 Neuman, J., Nowak, J., Huey, L., Burkholder, J., Dibb, J., Holloway, J., Liao, J., Peischl, J., Roberts, J., Ryerson, T., Scheuer,
747 E., Stark, H., Stickel, R., Tanner, D., and Weinheimer, A.: Bromine measurements in ozone depleted air over the Arctic Ocean,
748 *ATMOSPHERIC CHEMISTRY AND PHYSICS*, 10, 6503-6514, 10.5194/acp-10-6503-2010, 2010.

749 O'Dowd, C., Hämeri, K., Mäkelä, J., Väkeva, M., Aalto, P., de Leeuw, G., Kunz, G., Becker, E., Hansson, H., Allen, A.,
750 Harrison, R., Berresheim, H., Geever, M., Jennings, S., and Kulmala, M.: Coastal new particle formation: Environmental
751 conditions and aerosol physicochemical characteristics during nucleation bursts -: art. no. 8107, *JOURNAL OF*
752 *GEOPHYSICAL RESEARCH-ATMOSPHERES*, 107, 10.1029/2000JD000206, 2002.

753 Peng, X., Wang, T., Wang, W., Ravishankara, A., George, C., Xia, M., Cai, M., Li, Q., Salvador, C., Lau, C., Lyu, X., Poon,
754 C., Mellouki, A., Mu, Y., Hallquist, M., Saiz-Lopez, A., Guo, H., Herrmann, H., Yu, C., ..., and Chen, J.: Photodissociation of
755 particulate nitrate as a source of daytime tropospheric Cl₂, *NATURE COMMUNICATIONS*, 13,
756 10.1038/s41467-022-28383-9, 2022.

757 Peters, C., Pechtl, S., Stutz, J., Hebestreit, K., Hönninger, G., Heumann, K., Schwarz, A., Winterlik, J., and Platt, U.: Reactive
758 and organic halogen species in three different European coastal environments, *ATMOSPHERIC CHEMISTRY AND*
759 *PHYSICS*, 5, 3357-3375, 2005.

760 Pound, R., Brown, L., Evans, M., and Carpenter, L.: An improved estimate of inorganic iodine emissions from the ocean using
761 a coupled surface microlayer box model, *ATMOSPHERIC CHEMISTRY AND PHYSICS*, 24, 9899-9921, 10.5194/acp-24-
762 9899-2024, 2024.

763 Pound, R., Durcan, D., Evans, M., and Carpenter, L.: Comparing the Importance of Iodine and Isoprene on Tropospheric
764 Photochemistry, *GEOPHYSICAL RESEARCH LETTERS*, 50, 10.1029/2022GL100997, 2023.

765 Prados-Roman, C., Cuevas, C., Hay, T., Fernandez, R., Mahajan, A., Royer, S., Galí, M., Simó, R., Dachs, J., Grossmann, K.,
766 Kinnison, D., Lamarque, J., and Saiz-Lopez, A.: Iodine oxide in the global marine boundary layer, *ATMOSPHERIC
767 CHEMISTRY AND PHYSICS*, 15, 583-593, 10.5194/acp-15-583-2015, 2015.

768 Priestley, M., le Breton, M., Bannan, T., Worrall, S., Bacak, A., Smedley, A., Reyes-Villegas, E., Mehra, A., Allan, J., Webb,
769 A., Shallcross, D., Coe, H., and Percival, C.: Observations of organic and inorganic chlorinated compounds and their
770 contribution to chlorine radical concentrations in an urban environment in northern Europe during the wintertime,
771 *ATMOSPHERIC CHEMISTRY AND PHYSICS*, 18, 13481-13493, 10.5194/acp-18-13481-2018, 2018.

772 Pritchard, B., Altarawy, D., Didier, B., Gibson, T., and Windus, T.: New Basis Set Exchange: An Open, Up-to-Date Resource
773 for the Molecular Sciences Community, *JOURNAL OF CHEMICAL INFORMATION AND MODELING*, 59, 4814-4820,
774 10.1021/acs.jcim.9b00725, 2019.

775 Raso, A., Custard, K., May, N., Tanner, D., Newburn, M., Walker, L., Moore, R., Huey, L., Alexander, L., Shepson, P., and
776 Pratt, K.: Active molecular iodine photochemistry in the Arctic, *PROCEEDINGS OF THE NATIONAL ACADEMY OF
777 SCIENCES OF THE UNITED STATES OF AMERICA*, 114, 10053-10058, 10.1073/pnas.1702803114, 2017.

778 Read, K. A., Mahajan, A. S., Carpenter, L. J., Evans, M. J., Faria, B. V. E., Heard, D. E., Hopkins, J. R., Lee, J. D., Moller, S.
779 J., Lewis, A. C., Mendes, L., McQuaid, J. B., Oetjen, H., Saiz-Lopez, A., Pilling, M. J., and Plane, J. M. C.: Extensive halogen-
780 mediated ozone destruction over the tropical Atlantic Ocean, *Nature*, 453, 1232-1235, 10.1038/nature07035, 2008.

781 Reza, M., Iezzi, L., Finkenzeller, H., Roose, A., Ammann, M., and Volkamer, R.: Iodine Activation from Iodate Reduction in
782 Aqueous Films via Photocatalyzed and Dark Reactions, *ACS EARTH AND SPACE CHEMISTRY*, 8, 2495-2508,
783 10.1021/acsearthspacechem.4c00224, 2024.

784 Rice, O. K. and Ramsperger, H. C.: Theories of unimolecular gas reactions at low pressures, *Journal of the American Chemical
785 Society*, 49, 1617-1629, 10.1021/ja01406a001, 1927.

786 Rissanen, M., Mikkilä, J., Iyer, S., and Hakala, J.: Multi-scheme chemical ionization inlet (MION) for fast switching of reagent
787 ion chemistry in atmospheric pressure chemical ionization mass spectrometry (CIMS) applications, *ATMOSPHERIC
788 MEASUREMENT TECHNIQUES*, 12, 6635-6646, 10.5194/amt-12-6635-2019, 2019.

789 Riva, M., Pospisilova, V., Frege, C., Perrier, S., Bansal, P., Jorga, S., Sturm, P., Thornton, J., Rohner, U., and Lopez-Hilfiker,
790 F.: Evaluation of a reduced-pressure chemical ion reactor utilizing adduct ionization for the detection of gaseous organic and
791 inorganic species, *ATMOSPHERIC MEASUREMENT TECHNIQUES*, 17, 5887-5901, 10.5194/amt-17-5887-2024, 2024.

792 Robinson, M., Neuman, J., Huey, L., Roberts, J., Brown, S., and Veres, P.: Temperature-dependent sensitivity of iodide
793 chemical ionization mass spectrometers, *ATMOSPHERIC MEASUREMENT TECHNIQUES*, 15, 4295-4305, 10.5194/amt-
794 15-4295-2022, 2022.

795 Roscoe, H., Brough, N., Jones, A., Wittrock, F., Richter, A., Van Roozendael, M., and Hendrick, F.: Characterisation of vertical
796 BrO distribution during events of enhanced tropospheric BrO in Antarctica, from combined remote and in-situ measurements,
797 *JOURNAL OF QUANTITATIVE SPECTROSCOPY & RADIATIVE TRANSFER*, 138, 70-81, 10.1016/j.jqsrt.2014.01.026,
798 2014.

799 Saiz-Lopez, A. and Plane, J.: Novel iodine chemistry in the marine boundary layer, *GEOPHYSICAL RESEARCH LETTERS*,
800 31, 10.1029/2003GL019215, 2004.

801 Saiz-Lopez, A. and von Glasow, R.: Reactive halogen chemistry in the troposphere, *CHEMICAL SOCIETY REVIEWS*, 41,
802 6448-6472, 10.1039/c2cs35208g, 2012.

803 Saiz-Lopez, A., Fernandez, R. P., Ordonez, C., Kinnison, D. E., Martin, J. C. G., Lamarque, J. F., and Tilmes, S.: Iodine
804 chemistry in the troposphere and its effect on ozone, *Atmospheric Chemistry and Physics*, 14, 13119-13143, 10.5194/acp-14-
805 13119-2014, 2014.

806 Saiz-Lopez, A., Plane, J. M. C., Baker, A. R., Carpenter, L. J., von Glasow, R., Martin, J. C. G., McFiggans, G., and Saunders,
807 R. W.: Atmospheric Chemistry of Iodine, *Chemical Reviews*, 112, 1773-1804, 10.1021/cr200029u, 2012.

808 Sanchez, J., Tanner, D., Chen, D., Huey, L., and Ng, N.: A new technique for the direct detection of HO₂ radicals
809 using bromide chemical ionization mass spectrometry (Br-CIMS): initial characterization, *ATMOSPHERIC*
810 *MEASUREMENT TECHNIQUES*, 9, 3851-3861, 10.5194/amt-9-3851-2016, 2016.

811 Shaw, M. and Carpenter, L.: Modification of Ozone Deposition and I₂ Emissions at the Air-Aqueous Interface by Dissolved
812 Organic Carbon of Marine Origin, *ENVIRONMENTAL SCIENCE & TECHNOLOGY*, 47, 10947-10954,
813 10.1021/es4011459, 2013.

814 Sherwen, T., Evans, M. J., Carpenter, L. J., Andrews, S. J., Lidster, R. T., Dix, B., Koenig, T. K., Sinreich, R., Ortega, I.,
815 Volkamer, R., Saiz-Lopez, A., Prados-Roman, C., Mahajan, A. S., and Ordonez, C.: Iodine's impact on tropospheric oxidants:
816 a global model study in GEOS-Chem, *Atmospheric Chemistry and Physics*, 16, 1161-1186, 10.5194/acp-16-1161-2016,
817 2016a.

818 Sherwen, T., Schmidt, J., Evans, M., Carpenter, L., Grossmann, K., Eastham, S., Jacob, D., Dix, B., Koenig, T., Sinreich, R.,
819 Ortega, I., Volkamer, R., Saiz-Lopez, A., Prados-Roman, C., Mahajan, A., and Ordóñez, C.: Global impacts of tropospheric
820 halogens (Cl, Br, I) on oxidants and composition in GEOS-Chem, *ATMOSPHERIC CHEMISTRY AND PHYSICS*, 16,
821 12239-12271, 10.5194/acp-16-12239-2016, 2016b.

822 Simpson, W. R., Brown, S. S., Saiz-Lopez, A., Thornton, J. A., and von Glasow, R.: Tropospheric Halogen Chemistry:
823 Sources, Cycling, and Impacts, *Chemical Reviews*, 115, 4035-4062, 10.1021/cr5006638, 2015.

824 Sipilä, M., Sarnela, N., Jokinen, T., Henschel, H., Junninen, H., Kontkanen, J., Richters, S., Kangasluoma, J., Franchin, A.,
825 Peräkylä, O., Rissanen, M., Ehn, M., Vehkamäki, H., Kurten, T., Berndt, T., Petäjä, T., Worsnop, D., Ceburnis, D., Kerminen,
826 V., ..., and O'Dowd, C.: Molecular-scale evidence of aerosol particle formation via sequential addition of HIO₃,
827 *NATURE*, 537, 532-534, 10.1038/nature19314, 2016.

828 Sjostedt, S. and Abbatt, J.: Release of gas-phase halogens from sodium halide substrates: heterogeneous oxidation of frozen
829 solutions and desiccated salts by hydroxyl radicals, *ENVIRONMENTAL RESEARCH LETTERS*, 3, 10.1088/1748-
830 9326/3/4/045007, 2008.

831 SOLOMON, S., GARCIA, R., and RAVISHANKARA, A.: ON THE ROLE OF IODINE IN OZONE DEPLETION,
832 *JOURNAL OF GEOPHYSICAL RESEARCH-ATMOSPHERES*, 99, 20491-20499, 1994.

833 Stark, H., Yatayelli, R., Thompson, S., Kimmel, J., Cubison, M., Chhabra, P., Canagaratna, M., Jayne, J., Worsnop, D., and
834 Jimenez, J.: Methods to extract molecular and bulk chemical information from series of complex mass spectra with limited
835 mass resolution, *INTERNATIONAL JOURNAL OF MASS SPECTROMETRY*, 389, 26-38, 10.1016/j.ijms.2015.08.011,
836 2015.

837 Tham, Y. J., He, X. C., Li, Q. Y., Cuevas, C. A., Shen, J. L., Kalliokoski, J., Yan, C., Iyer, S., Lehmusjarvi, T., Jang, S. H.,
838 Thakur, R. C., Beck, L., Kemppainen, D., Olin, M., Sarnela, N., Mikkila, J., Hakala, J., Marbouti, M., Yao, L., ..., and Sipilä,
839 M.: Direct field evidence of autocatalytic iodine release from atmospheric aerosol, *Proceedings of the National Academy of*
840 *Sciences of the United States of America*, 118, 8, 10.1073/pnas.2009951118, 2021.

841 Vogt, R., Sander, R., Von Glasow, R., and Crutzen, P.: Iodine chemistry and its role in halogen activation and ozone loss in
842 the marine boundary layer: A model study, *JOURNAL OF ATMOSPHERIC CHEMISTRY*, 32, 375-395,
843 10.1023/A:1006179901037, 1999.

844 Wang, M., Kong, W., Marten, R., He, X., Chen, D., Pfeifer, J., Heitto, A., Kontkanen, J., Dada, L., Kurten, A., Yli-Juuti, T.,
845 Manninen, H., Amanatidis, S., Amorim, A., Baalbaki, R., Baccarini, A., Bell, D., Bertozzi, B., Bräkling, S., ..., and Donahue,
846 N.: Rapid growth of new atmospheric particles by nitric acid and ammonia condensation, *NATURE*, 581, 184-+,
847 10.1038/s41586-020-2270-4, 2020.

848 Wang, M. Y., He, X. C., Finkenzeller, H., Iyer, S., Chen, D. X., Shen, J. L., Simon, M., Hofbauer, V., Kirkby, J., Curtius, J.,
849 Maier, N., Kurtén, T., Worsnop, D. R., Kulmala, M., Rissanen, M., Volkamer, R., Tham, Y. J., Donahue, N. M., and Sipilä,
850 M.: Measurement of iodine species and sulfuric acid using bromide chemical ionization mass spectrometers, *Atmospheric*
851 *Measurement Techniques*, 14, 4187-4202, 10.5194/amt-14-4187-2021, 2021a.

852 Wang, X., Jacob, D., Downs, W., Zhai, S., Zhu, L., Shah, V., Holmes, C., Sherwen, T., Alexander, B., Evans, M., Eastham,
853 S., Neuman, J., Veres, P., Koenig, T., Volkamer, R., Huey, L., Bannan, T., Percival, C., Lee, B., and Thornton, J.: Global
854 tropospheric halogen (Cl, Br, I) chemistry and its impact on oxidants, *ATMOSPHERIC CHEMISTRY AND PHYSICS*, 21,
855 13973-13996, 10.5194/acp-21-13973-2021, 2021b.

856 Yeoman, A., Heeley-Hill, A., Shaw, M., Andrews, S., and Lewis, A.: Inhalation of VOCs from facial moisturizers and the
857 influence of dose proximity, *INDOOR AIR*, 32, 10.1111/ina.12948, 2022.

858 Zhang, Y., Liu, R., Yang, D., Guo, Y., Li, M., and Hou, K.: Chemical ionization mass spectrometry: Developments and
859 applications for on-line characterization of atmospheric aerosols and trace gases, TRAC-TRENDS IN ANALYTICAL
860 CHEMISTRY, 168, 10.1016/j.trac.2023.117353, 2023.

861